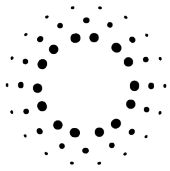

IFT - UNESP
INSTITUTO DE FÍSICA TEÓRICA

Master's Dissertation IFT–T.006/2025

Dynamic behavior of an active particle embedded in a smectic liquid crystal

Yhony Mamani Arce

Advisor

Danilo Liarte

July 2025

Mamani Arce, Yhony
M263d Dynamic behavior of an active particle embedded in a smectic liquid crystal / Yhony Mamani Arce. – São Paulo, 2025
75 f: il. color.

Dissertação (mestrado) – Universidade Estadual Paulista (Unesp), Instituto de Física Teórica (IFT), São Paulo
Orientador: Danilo Liarte

1. Física. 2. Física teórica. 3. Matéria condensada. I. Título

Sistema de geração automática de fichas catalográficas da Unesp. Biblioteca do Instituto de Física Teórica (IFT), São Paulo. Dados fornecidos pelo autor(a).

DYNAMIC BEHAVIOR OF AN ACTIVE PARTICLE EMBEDDED IN A SMECTIC LIQUID CRYSTAL

Dissertação de Mestrado apresentada ao Instituto de Física Teórica do Câmpus de São Paulo, da Universidade Estadual Paulista "Júlio de Mesquita Filho", como parte dos requisitos para obtenção do título Mestre em Ciências, área: Física.

Comissão Examinadora:

Prof. Dr. DANILO BARBOSA LIARTE (Orientador)
Instituto de Física Teórica/UNESP

Prof. Dr. ALEXANDRE REILY ROCHA
Instituto de Física Teórica/UNESP

Prof. Dr. SILVIO ROBERTO DE AZEVEDO SALINAS
Instituto de Física/Universidade de São Paulo

Conceito: Aprovado

São Paulo, 09 de julho de 2025.

To my mom Hilda and dad Domingo

...

Acknowledgements

I would like to take this opportunity to express my sincere gratitude to all those who, in one way or another, accompanied and supported me throughout this challenging and enriching journey. These words may fall short in naming everyone who contributed to this process, and if I happen to leave someone out, I kindly ask for your understanding and offer my heartfelt thanks.

First and foremost, I am deeply grateful to my advisor, Prof. Danilo Liarte, for his constant guidance, support, and trust throughout this research. His insight and encouragement were fundamental at every stage of this work. I also want to thank William Oropesa for the many valuable discussions about the simulations, and André Vieira from USP for the helpful conversations that shaped the theoretical formulation. Their contributions greatly enriched this project.

I am also thankful to CNPq for providing the financial support through a master's scholarship, which made it possible for me to pursue my studies in Brazil.

To my colleagues at IFT, I thank you for the lunchtime conversations, full of spontaneous ideas, laughter, and friendship. These everyday moments helped lighten the intensity of academic life and brought much-needed joy. I also want to express my appreciation to the friends I met through the Volunteer League here in São Paulo, whose spirit of solidarity and kindness inspired me and made my time here even more meaningful.

A very special thanks goes to my lifelong friends Ivan H., Marvin A. and Milagros L., for their unconditional support and friendship over the years.

Finally, I am deeply thankful to my parents and siblings for their unwavering love, trust, and encouragement throughout my life. Their constant support, both emotional and moral, gave me the strength to persevere during difficult times and celebrate the good ones. This achievement would not have been possible without their presence, even from afar.

This work is not only the result of scientific effort but also of the collective support, collaboration, and companionship of everyone mentioned above. To all of you, thank you from the bottom of my heart.

Kaiq'its juta?
K'unats akan'ta?
K'aiqirus sarta?

D.&H.

Resumo

Sistemas de matéria ativa, que consomem energia continuamente para gerar movimento direcionado, exibem fenômenos emergentes fascinantes. Embora sua dinâmica em fluidos isotrópicos seja bem compreendida, seu comportamento em ambientes complexos e anisotrópicos permanece uma fronteira de pesquisa. Esta dissertação investiga as propriedades de transporte de partículas brownianas ativas (ABPs) em ambientes de cristal líquido esmético-A (SmA), com foco específico em configurações uniformes e aquelas estruturadas por Domínios Cônicos Focais (FCDs). Empregamos simulações numéricas para analisar o deslocamento quadrático médio (MSD), incluindo seus componentes total, paralelo e perpendicular, e o deslocamento quadrático médio rotacional (RMSD) de ABPs. Em uma configuração SmA "quase plana", nossos resultados confirmam o comportamento característico de ABPs, mostrando uma transição de movimento balístico para movimento difusivo mais intenso, onde a velocidade de autopropulsão determina o coeficiente de difusão efetivo. O acoplamento entre o alinhamento entre a ABP e o campo diretor uniforme influencia significativamente a persistência, enquanto o MSD perpendicular permanece puramente difusivo, consistente com um meio rígido e não deformável. A introdução de FCDs *miméticos* leva a uma dinâmica mais complexa. As singularidades dos FCDs são identificadas como centros de reorientação eficazes, onde o campo diretor local fica sujeito a uma mudança rápida e a natureza quadrática da interação de alinhamento levam à reorientação estocástica das ABPs. Consequentemente, o MSD perpendicular exibe um regime superdifusivo transiente em tempos curtos, atribuído ao movimento persistente da partícula dentro de um perfil curvo dos diretores. De forma mais notável, o MSD paralelo exibe um comportamento oscilatório intrigante em regimes de tempos intermediários e longos. O RMSD reflete qualitativamente a interação entre ruído rotacional e o termo de alinhamento, com os FCDs contribuindo para as orientações aleatórias, em geral. Este trabalho destaca a influência profunda de estruturas líquido-cristalinas complexas no transporte de matéria ativa. Nossas descobertas fornecem insights fundamentais sobre como a heterogeneidade espacial em sistemas de matéria mole pode ser aproveitada para controlar e manipular a dinâmica de agentes ativos, com implicações para a microrrobótica e a projeção de materiais ativos.

Palavras Chaves: Partículas Brownianas Ativas; Smectic-A; Domínios Cônicos Focais; Deslocamento Quadrático Médio; Transporte Anisotrópico.

Áreas do conhecimento: Física; Física Teórica; Física da Matéria Condensada; Matéria Ativa.

Abstract

Active matter systems, which continuously consume energy to generate directed motion, exhibit fascinating emergent phenomena. While their dynamics in isotropic fluids are well-understood, their behavior in complex, anisotropic environments remains a frontier of research. This dissertation investigates the transport properties of active Brownian particles (ABPs) in smectic-A (SmA) liquid crystal environments, specifically focusing on uniform configurations and those structured by Focal Conic Domains (FCDs). We employ numerical simulations to analyze the mean squared displacement (MSD), including its total, parallel, and perpendicular components, and the rotational mean squared displacement (RMSD) of ABPs. In a nearly flat SmA configuration, our results confirm characteristic ABP behavior, showing a transition from ballistic to enhanced diffusive motion, where the self-propulsion velocity dictates the effective diffusion coefficient. The alignment coupling between the ABP and the uniform director field significantly influences persistence, while the perpendicular MSD remains purely diffusive, consistent with a rigid, non-deformable medium. The introduction of mimetic FCDs leads to a more intricate dynamics. FCD singularities are identified as effective reorientation centers, where the rapidly changing local director field and the quadratic nature of the alignment interaction lead to stochastic reorientation of the ABPs. Consequently, the perpendicular MSD exhibits a transient superdiffusive regime at short times, attributed to the particle's persistent motion within a curving director landscape. Most notably, the parallel MSD displays a remarkable oscillatory behavior at intermediate to long times. The RMSD qualitatively reflects the interplay of rotational noise and alignment, with FCDs contributing to the overall random orientations. This work underscores the profound influence of complex, liquid crystalline architectures on active matter transport. Our findings provide fundamental insights into how spatial heterogeneity in soft matter systems can be leveraged to control and manipulate the dynamics of active agents, with implications for micro-robotics and active material design.

Keywords: Active Brownian Particles; Smectic-A; Focal Conic Domains; Mean Squared Displacement; Anisotropic Transport.

Knowledge areas: Physics; Theoretical Physics; Condensed Matter Physics; Active Matter.

Contents

Chapter 1

Introduction

The natural world is teeming with systems that consume energy at the microscopic level to generate directed motion and exert forces, collectively known as active matter [20, 21]. Unlike traditional equilibrium systems governed by thermal fluctuations and energy minimization, active matter operates fundamentally out of equilibrium. These systems continuously dissipate energy to perform work, leading to fascinating emergent phenomena, such as collective motion, self-organization into intricate patterns, enhanced diffusion, and anomalous transport properties [3]. Examples range from living biological systems like swimming bacteria (e.g., *E. coli*), motile cells (e.g., spermatozoa, immune cells), and bird flocks to synthetic systems, including self-propelled colloidal particles, active emulsions, and catalytic microswimmers [18]. The study of active matter transcends traditional disciplinary boundaries, drawing insights from physics, biology, chemistry, and engineering, with implications for designing smart materials, micro-robotics, and understanding biological processes.

A central theme in active matter research is understanding how individual microscopic activity translates into macroscopic behavior. While significant progress has been made in characterizing active particles in simple, isotropic fluids, many natural and artificial environments are inherently complex, heterogeneous, and anisotropic. Such environments can dramatically alter the transport, self-assembly, and collective dynamics of active agents, leading to novel behaviors not observed in bulk, homogeneous conditions. Examples of such complex environments include porous media, crowded cellular environments, interfaces, and ordered soft materials [3].

Among the most compelling and experimentally accessible complex environments are liquid crystals. These fascinating states of matter bridge the gap between conventional isotropic liquids and crystalline solids, possessing both fluidity and long-range order [10, 9]. Their anisotropic molecular building blocks self-organize into phases with distinct orientational and/or positional order, characterized by a macroscopic average orientation, known as the director field ($\hat{\mathbf{n}}$). This inherent

anisotropy makes liquid crystals ideal platforms for studying active matter, as they provide a spatially varying, ordered landscape that can guide, confine, or channel the motion of active particles.

Of particular interest for this thesis is the smectic-A (SmA) liquid crystal phase. In the SmA phase, elongated molecules spontaneously arrange into distinct, well-defined layers, while remaining liquid-like within these layers. The average molecular orientation is, on average, perpendicular to these layers, meaning the director $\hat{\mathbf{n}}$ locally aligns with the layer normal [10]. This one-dimensional positional order, coupled with orientational order, endows SmA phases with unique elastic properties. They resist compression and stretching of their layers (characterized by the elastic constant B) and bending (splay) distortions of their layers (characterized by K_1), while allowing easy flow within the layers. This combination of fluidity and layered elasticity makes SmA a highly non-trivial medium for active particles.

While ideal SmA phases consist of flat, parallel layers, in reality, they often form complex, spatially varying structures to accommodate boundary conditions, external fields, or topological necessities. Among the most iconic and ubiquitous of these structures are Focal Conic Domains (FCDs) [15]. FCDs are thermodynamically stable patterns of curved layers that arise from the unique elastic properties of smectics. They are characterized by smectic layers arranged as portions of *Dupin cyclides*, whose normals (and thus the local director) point towards two orthogonal focal curves: an ellipse and a hyperbola.

The presence of FCDs introduces a highly heterogeneous and spatially varying director field into the smectic environment. These domains are rich in curvature and contain intrinsic singularities (focal lines or points) where the director field is ill-defined or undergoes abrupt changes. Such regions are known to act as traps or reorientation centers for various entities, including passive particles or light. For active particles, these structured environments offer a fascinating landscape where the inherent self-propulsion and alignment tendencies of the particles interact with the pre-existing geometrical features of the liquid crystal.

1.1 Research Gap and Objectives

Despite growing interest in active matter in complex environments, the dynamics of active Brownian particles navigating through the intricate, director fields of FCDs in smectic-A liquid crystals remain underexplored. While some studies

have examined active particles in simpler nematic textures or deformable smectics [25, 12], a systematic investigation into how the unique geometry, curvature, and singularities of FCDs influence the anisotropic transport of ABPs is lacking. Understanding this interplay is crucial for both fundamental physics (revealing novel non-equilibrium phenomena) and potential applications (e.g., guided transport of micro-robots in structured soft media).

On the experimental front, recent studies in nematic liquid crystals and lyotropic chromonic liquid crystals have successfully demonstrated the guided motion of motile bacteria and synthetic microswimmers along a pre-defined director field, revealing how anisotropic environments can rectify and channel active motion [2, 23, 26, 31]. These experiments, often using high-speed microscopy and patterned liquid crystal cells, have been used to describe phenomena such as controlled cargo transport along the director and the ability of active particles to act as tracers of the complex director profile [26]. However, these results focus either on less structured nematic phases or on simple smectic geometries. The unique challenge lies in preparing stable and reproducible smectic textures, such as Focal Conic Domains, in a cell suitable for high-resolution particle tracking. The numerical results presented in this thesis provide theoretical predictions that can guide future experimental design, which would be crucial for validating our theoretical framework and advancing the understanding of active matter in the unique, intricate landscape of smectic liquid crystals.

The results presented here aim to bridge this gap by means of an analysis of numerical simulations for the dynamics of active particles embedded in the complex microstructure of smectic-A environments. Our primary goals are:

1. To characterize the transport properties of ABPs in a nearly uniform SmA configuration, establishing a baseline for understanding their behavior in anisotropic media.

2. To investigate how the complex, spatially varying director field and singularities of *mimetic* FCDs affect the ABP dynamics, particularly their translational and rotational movement.

3. To quantify the anisotropic Mean Squared Displacement (MSD), distinguishing between components parallel and perpendicular to the local smectic director, to reveal the channeling and scattering effects of the mimetic FCDs.

4. To identify and explain any anomalous transport phenomena (e.g., superdif-

fusive, subdiffusive) that emerge due to the interaction of ABPs with FCDs.

5. To provide a robust numerical framework for simulating active particles in such complex liquid crystalline environments.

1.2 Dissertation Structure

This dissertation contain five chapters that provide the basis to address the aforementioned objectives:

- **Chapter 1: Introduction** provides a general overview of active matter and liquid crystals, highlights the importance of studying active particles in complex anisotropic environments, outlines the specific problem addressed by this work, and gives details of the dissertation objectives.
- **Chapter 2: Active Matter** delves into the theoretical foundations of active matter. It introduces the concepts of passive and active Brownian motion, derives the governing Langevin equations for active Brownian particles, and discusses their characteristic transport properties in simple isotropic media.
- **Chapter 3: Liquid Crystals** provides a comprehensive overview of liquid crystal physics. It describes the fundamental properties and phases of liquid crystals, with a particular focus on the smectic-A phase. Crucially, this chapter explains the fundamentals of FCDs. It also clarifies how the director field data for FCDs that will be used in our simulations originates in existing computational work [17].
- **Chapter 4: Results and Analysis** presents the core of our new numerical results. It gives details of the equations of motion for ABPs in the smectic environment, describes the simulation algorithm, and explains the methods used to analyze the particle trajectories, including the calculation of anisotropic MSD components. This chapter then presents and discusses the key results for ABPs in both flat and mimetic-FCD-structured SmA configurations.
- **Chapter 5: Conclusions and Outlook** summarizes the main findings of this thesis, reiterates their significance, and proposes future research directions that naturally extend from the present work.

Through this systematic investigation, we aim to contribute to a deeper understanding of active matter physics in complex, structured environments, particularly relevant for soft matter systems and micro-scale active transport phenomena.

Chapter 2

Active Matter

This chapter provides a brief introduction to active matter, focusing on a few paradigmatic models and their physical behavior. We delve into the essential concepts of both passive and active Brownian particles, crucial for understanding the stochastic dynamics that underpin our study of active swimmers in smectic liquid crystals. Our general treatment of stochastic processes and Brownian motion draws extensively from classical texts on stochastic dynamics [24, 27], while the broader context of active matter models is based on references [21, 3]. Our discussion of two-dimensional active Brownian motion follows the established framework reviewed by Bechinger et al. [3].

2.1 Introduction

The realm of active matter comprises systems composed of individual units capable of continuously converting stored or ambient energy into systematic, directed motion or mechanical work at the microscopic level [3, 11, 20]. This fundamental ability to break time-reversal symmetry locally, by consuming energy to generate self-propulsion forces, distinguishes active matter from conventional passive systems that typically tend towards thermodynamic equilibrium [21]. Unlike passive Brownian systems, whose behavior is governed by equilibrium statistical mechanics and characterized by a precise balance between thermal fluctuations and energy dissipation [27], active systems are intrinsically driven out of equilibrium. This continuous energy input at the constituent level leads to fascinating emergent phenomena, such as self-organization, collective motion (like flocking and swarming) [28], pattern formation, and unique mechanical properties.

The study of active matter spans an impressive range of scales, from biological microorganisms to macroscopic assemblies, and encompasses both living and artificial entities [3]. On the biological front, examples include microorganisms like

bacteria and algae that propel themselves through fluids, forming dynamic structures such as vortices [1] and fractal clusters [22]. At larger scales, the collective behavior of animal groups like flocks of birds, schools of fish, and colonies of ants demonstrates intricate self-organization driven by individual active movements and local interactions [4]. Beyond biological systems, synthetic active matter has seen rapid development. Examples range from anisotropic nanoparticles driven by localized thermal gradients, to chemically propelled colloids (often termed Janus particles due to their asymmetric design), and even vertically vibrated granular materials that exhibit collective motion. The ability of these synthetic systems to mimic complex biological behaviors, such as directed search (e.g., Janus microparticles targeting bacteria), underscores the potential for technological innovation in designing adaptive materials and micro-robots [30].

From a theoretical physics perspective, the hallmark of active matter lies in its non-equilibrium nature. The continuous local energy injection means that the system's dynamics cannot be described by equilibrium ensembles or a global free energy minimization principle. Instead, active systems perpetually dissipate energy into their environment, leading to a steady state that is fundamentally non-Boltzmannian [20]. This absence of detailed balance and time-reversal symmetry imposes significant challenges but also opens new avenues for theoretical modeling and statistical mechanics.

The modeling of active matter typically involves coarse-graining microscopic details to capture the essential physical principles. At a fundamental level, active matter systems are composed of discrete active particles. A common and insightful approach involves modeling individual particles "subject to" a constant *self-propulsion force*, $\vec{f}_{act}$, or possessing a constant *self-propulsion speed*, v_s, whose direction, $\hat{u}$, evolves stochastically or deterministically in response to the environment. These effective parameters represent the continuous local energy input that drives the system out of equilibrium. The rotational dynamics governing the direction $\hat{u}$ is crucial for determining the overall behavior and gives rise to different canonical models of active matter, such as *Active Brownian Particles* (ABPs) and Run-and-Tumble Particles (RTPs) [3]. These microscopic models, despite their conceptual simplicity, have provided profound insights into collective behaviors like *motility-induced phase separation* (MIPS) and particle accumulation at boundaries, which have been experimentally validated [8].

In the following sections, we will delve deeper into the fundamental models used to describe active particle dynamics. We will first review *passive Brownian*

motion as a foundational concept in stochastic processes and statistical mechanics, establishing the equilibrium benchmark. We will then introduce the *Active Brownian Particle* (ABP) model, building upon the principles of Brownian motion but incorporating the non-equilibrium self-propulsion force and its associated dynamics. This will lay the groundwork for understanding the more complex behavior of active particles in structured environments, such as the smectic phases discussed in this thesis.

2.2 Brownian Motion: From Thermal Fluctuations to Active Propulsion

Brownian motion, first observed by botanist Robert Brown in 1827, refers to the erratic, seemingly random movement of microscopic particles suspended in a fluid. Brown's initial observations, made with pollen grains in water, were crucial. He meticulously confirmed that this motion was not biological by observing similar behavior in ancient water trapped within quartz [6], indicating a purely physical origin. The true nature of this phenomenon remained a mystery until 1905, when Albert Einstein, William Sutherland, and Marian von Smoluchowski independently provided a theoretical explanation. They proposed that this seemingly random motion results from the incessant and random collisions between the much smaller, unobservable fluid molecules (e.g., water molecules) and the larger, visible Brownian particle. This groundbreaking theory, which provided compelling evidence for the atomic and molecular nature of matter, was experimentally validated by Jean Baptiste Perrin, who earned the 1926 Nobel Prize in Physics for his work. Since then, the study of Brownian motion has been fundamental, driving advancements across diverse fields, including equilibrium and non-equilibrium statistical physics [16, 14], fluid mechanics, and the mathematical foundations of probability and stochastic modeling [13]. More recently, it has become pivotal in studies of soft matter, biophysics, active matter [3], and even quantum fluctuations [19].

The description of a particle undergoing Brownian motion is often captured by the Langevin equation. This stochastic differential equation provides a coarse-grained statistical description of the particle's dynamics by accounting for the averaged effects of countless collisions with surrounding fluid molecules, as well as any external or internal forces acting on the particle.

For a particle of mass m experiencing a general potential $U(\vec{r})$ and an active self-propulsion force $\vec{f}_{\text{act}}$, the Langevin equation in its full form is:

$$m\frac{d\vec{v}}{dt} = -\gamma\frac{d\vec{r}}{dt} - \nabla U(\vec{r}) + \vec{f}_{\text{act}} + \vec{F}(t). \tag{2.1}$$

Let's clarify the meaning of each term in this equation, which forms the basis for understanding both passive and active particle dynamics:

- $m\frac{d\vec{v}}{dt}$: This is the inertial term, representing the product of the particle's mass m and its acceleration $\frac{d\vec{v}}{dt}$. While important for macroscopic objects, for microscopic particles in viscous fluids, this term is often negligible due to the small mass and high damping, which will be discussed in the next section.

- $-\gamma\frac{d\vec{r}}{dt}$: This is the dissipative (friction) force, also known as Stokes' drag for spherical particles. It acts opposite to the velocity $\frac{d\vec{r}}{dt}$ and is proportional to it via the friction coefficient γ. This term represents the continuous energy loss to the fluid due to viscous interactions. In anisotropic media like liquid crystals, γ generally becomes a tensor, reflecting direction-dependent drag.

- $-\nabla U(\vec{r})$: This represents an external conservative force derived from a potential energy function $U(\vec{r})$. This could be a gravitational force, an optical trapping potential, or forces from physical boundaries.

- $\vec{f}_{\text{act}}$: This is the active force, a unique component for active matter. It represents the non-thermal, self-propelling drive of the particle, arising from its continuous, internal energy consumption (e.g., chemical reactions, conformational changes). Its specific form depends on the active particle model, but it is typically a persistent force that breaks thermal equilibrium.

- $\vec{F}(t)$: This is the stochastic (thermal) noise term, representing the random, instantaneous forces experienced by the particle due to incessant collisions with the surrounding fluid molecules. It is typically modeled as Gaussian white noise with zero mean,

$$\langle\vec{F}(t)\rangle = 0, \tag{2.2}$$

and variance

$$\langle F_i(t)F_j(t')\rangle = 2D_p\delta_{ij}\delta(t-t'), \quad i,j \in \{x,y,z\} \tag{2.3}$$

where δ_{ij} is the Kronecker delta (indicating that different components of the noise are uncorrelated) and $\delta(t - t')$ is the Dirac delta function (signifying that the noise is uncorrelated at different times, characteristic of white noise). The parameter D_p is the intensity of the noise associated with momentum fluctuations.

In thermal equilibrium, the fluctuation-dissipation theorem provides a crucial link between the friction coefficient γ and the noise intensity D_p. It states that the magnitude of the random thermal forces must be precisely balanced by the viscous drag force to maintain a constant average kinetic energy, in accordance with the equipartition theorem. Quantitatively, this relationship is given by:

$$D_p = k_B T \gamma \tag{2.4}$$

Where k_B is the Boltzmann constant and T is the absolute temperature of the surrounding thermal bath. This equation is a cornerstone of equilibrium statistical mechanics, asserting that dissipation and fluctuation are intrinsically linked in systems at thermal equilibrium.

2.2.1 Passive Brownian Motion (PBM)

Passive Brownian motion describes the stochastic motion of particles that do not consume internal energy for self-propulsion. Their dynamics are governed solely by interactions with the surrounding thermal bath and any external conservative forces. The Langevin equation for a passive Brownian particle simplifies to:

$$m\frac{d\vec{v}}{dt} = -\gamma\frac{d\vec{r}}{dt} - \nabla U(\vec{r}) + \vec{F}(t). \tag{2.5}$$

To simplify the Langevin equation, particularly for analysis of the particle's velocity, it's often convenient to divide Eq. (2.5) by the mass m:

$$\frac{d\vec{v}}{dt} = -\frac{\gamma}{m}\vec{v} - \frac{1}{m}\nabla U(\vec{r}) + \sqrt{2D}\vec{\zeta}(t) \tag{2.6}$$

where $\frac{1}{m}\vec{F}(t) = \sqrt{2D}\vec{\zeta}(t)$. Here, $\vec{\zeta}(t)$ is a new stochastic variable, representing normalized Gaussian white noise, with properties:

$$\langle\vec{\zeta}(t)\rangle = \vec{0} \tag{2.7}$$

$$\langle \zeta_i(t)\zeta_j(t')\rangle = \delta_{ij}\delta(t-t') \tag{2.8}$$

The parameter D is the noise intensity associated with velocity, related to D_p by $D = D_p/m^2$. Thus, from the fluctuation-dissipation theorem (Eq. 2.4), we find $D = \frac{k_B T\gamma}{m^2}$. The term $\tau_m = m/\gamma$ is often referred to as the momentum relaxation time or viscous relaxation time, representing the timescale over which the particle's velocity decays due to friction.

Underdamped Brownian Motion: Velocity Dynamics

For a free Brownian particle (i.e., in the absence of an external potential, $\nabla U(\vec{r}) = \vec{0}$), Eq. (2.6) simplifies to:

$$\frac{d\vec{v}}{dt} + \frac{\gamma}{m}\vec{v} = \sqrt{2D}\vec{\zeta}(t) \tag{2.9}$$

This is a first-order linear ordinary differential equation with a stochastic driving term. Its general solution can be obtained by integrating factors. First, consider the homogeneous (deterministic) part:

$$\frac{d\vec{v}}{dt} + \frac{\gamma}{m}\vec{v} = 0$$

The solution to this homogeneous equation describes the exponential decay of an initial velocity due to friction:

$$\vec{v}_{\text{homo}}(t) = \vec{v}(0)e^{-\frac{\gamma}{m}t} \tag{2.10}$$

To find the full solution, we multiply Eq. (2.9) by the integrating factor $e^{\frac{\gamma}{m}t}$:

$$e^{\frac{\gamma}{m}t}\frac{d\vec{v}}{dt} + \frac{\gamma}{m}e^{\frac{\gamma}{m}t}\vec{v} = \sqrt{2D}e^{\frac{\gamma}{m}t}\vec{\zeta}(t)$$
$$\frac{d}{dt}(e^{\frac{\gamma}{m}t}\vec{v}) = \sqrt{2D}e^{\frac{\gamma}{m}t}\vec{\zeta}(t)$$

Integrating from 0 to t:

$$e^{\frac{\gamma}{m}t}\vec{v}(t) - \vec{v}(0) = \sqrt{2D}\int_0^t e^{\frac{\gamma}{m}t'}\vec{\zeta}(t')dt'$$

Solving for $\vec{v}(t)$ yields the complete solution for the velocity of an underdamped Brownian particle:

$$\vec{v}(t) = e^{-\frac{\gamma}{m}t}\vec{v}(0) + \sqrt{2D}e^{-\frac{\gamma}{m}t}\int_0^t e^{\frac{\gamma}{m}t'}\vec{\zeta}(t')dt' \tag{2.11}$$

This solution shows that the velocity comprises two parts: a deterministic decay of the initial velocity and a stochastic contribution from the fluctuating force.

To understand the macroscopic behavior, we typically analyze the ensemble averages of relevant quantities. The mean velocity is straightforward:

$$\langle\vec{v}(t)\rangle = \langle e^{-\frac{\gamma}{m}t}\vec{v}(0) + \sqrt{2D}e^{-\frac{\gamma}{m}t}\int_0^t e^{\frac{\gamma}{m}t'}\vec{\zeta}(t')dt'\rangle \tag{2.12}$$

Since $\langle\vec{\zeta}(t')\rangle = \vec{0}$, the integral term vanishes upon averaging:

$$\langle\vec{v}(t)\rangle = \vec{v}(0)e^{-\frac{\gamma}{m}t} \tag{2.13}$$

This indicates that, on average, the particle's initial velocity decays exponentially to zero due to friction.

The mean squared velocity, $\langle v^2(t)\rangle$, provides insight into the kinetic energy of the particle. Starting from $(\vec{v}(t) - \langle\vec{v}(t)\rangle)^2$:

$$(\vec{v}(t) - \langle\vec{v}(t)\rangle)^2 = 2De^{-\frac{2\gamma}{m}t}\int_0^t\int_0^t e^{\frac{\gamma}{m}(t'+t'')}\vec{\zeta}(t')\cdot\vec{\zeta}(t'')dt'dt''$$

Averaging and utilizing the noise correlation property $\langle\zeta_i(t')\zeta_j(t'')\rangle = \delta_{ij}\delta(t'-t'')$:

$$\begin{aligned}
\langle v^2(t)\rangle - \langle\vec{v}(t)\rangle^2 =& 2De^{-\frac{2\gamma}{m}t}\int_0^t\int_0^t e^{\frac{\gamma}{m}(t'+t'')}\sum_{i=1}^{d}\delta_{ii}\delta(t'-t'')dt'dt'' \\
=& 2De^{-\frac{2\gamma}{m}t}d\int_0^t e^{\frac{2\gamma}{m}t'}dt' \\
=& 2De^{-\frac{2\gamma}{m}t}d\left[\frac{m}{2\gamma}e^{\frac{2\gamma}{m}t'}\right]_0^t \\
=& 2De^{-\frac{2\gamma}{m}t}d\frac{m}{2\gamma}(e^{\frac{2\gamma}{m}t}-1) \\
\langle v^2(t)\rangle - \langle\vec{v}(t)\rangle^2 =& \frac{Dm}{\gamma}d(1-e^{-\frac{2\gamma}{m}t})
\end{aligned}$$

Thus,

$$\langle v^2(t)\rangle = \langle \vec{v}(t)\rangle^2 + \frac{Dm}{\gamma} d(1 - e^{-\frac{2\gamma}{m}t}) \tag{2.14}$$

As $t \to \infty$, the particle reaches the stationary state (thermal equilibrium) where $\langle \vec{v}(t)\rangle \to \vec{0}$ and the exponential term vanishes. In this long-time limit, the mean squared velocity for each component v_i is:

$$\langle v_i^2\rangle = \frac{Dm}{\gamma} = \frac{k_B T}{m} \quad \text{for } i = 1, \ldots, d \tag{2.15}$$

This result is in perfect agreement with the equipartition theorem of classical statistical mechanics, which states that for each degree of freedom associated with quadratic energy dependence, the average energy is $\frac{1}{2}k_B T$. Since kinetic energy for each dimension is $\frac{1}{2}mv_i^2$, this implies $\langle \frac{1}{2}mv_i^2\rangle = \frac{1}{2}k_B T$, leading directly to $\langle v_i^2\rangle = \frac{k_B T}{m}$. This consistency further validates the Langevin equation as a microscopic description of Brownian motion at thermal equilibrium.

Mean Squared Displacement (MSD)

The Mean Squared Displacement (MSD), denoted as $\langle[\Delta\vec{r}(t)]^2\rangle$, is a key quantity for characterizing the diffusive behavior of particles. It measures the average squared distance a particle travels from its initial position over a time interval t.

$$\langle[\Delta\vec{r}(t)]^2\rangle = \langle|\vec{r}(t) - \vec{r}(0)|^2\rangle \tag{2.16}$$

The position of the particle $\vec{r}(t)$ is obtained by integrating its velocity:

$$\vec{r}(t) = \vec{r}(0) + \int_0^t \vec{v}(t')dt' \tag{2.17}$$

Substituting the full solution for $\vec{v}(t)$ from Eq. (2.11) into Eq. (2.17):

$$\begin{aligned}
\vec{r}(t) - \vec{r}(0) &= \int_0^t \left(e^{-\frac{\gamma}{m}t'}\vec{v}(0) + \sqrt{2D}e^{-\frac{\gamma}{m}t'} \int_0^{t'} e^{\frac{\gamma}{m}t''}\vec{\zeta}(t'')dt'' \right) dt' \\
&= \vec{v}(0) \int_0^t e^{-\frac{\gamma}{m}t'}dt' + \sqrt{2D} \int_0^t e^{-\frac{\gamma}{m}t'} \int_0^{t'} e^{\frac{\gamma}{m}t''}\vec{\zeta}(t'')dt''dt' \\
&= \vec{v}(0)\frac{m}{\gamma}(1 - e^{-\frac{\gamma}{m}t}) + \frac{m}{\gamma}\sqrt{2D} \int_0^t \vec{\zeta}(t'')(1 - e^{\frac{\gamma}{m}(t''-t)})dt''
\end{aligned}$$

The last step involves a change in the order of integration, which is a common technique for such integrals (Dirichlet's formula for changing limits).

Now, to calculate the MSD, we need to square this displacement and take the ensemble average:

$$\langle|\vec{r}(t)-\vec{r}(0)|^2\rangle = \left\langle \left| \vec{v}(0)\frac{m}{\gamma}(1-e^{-\frac{\gamma}{m}t}) + \frac{m}{\gamma}\sqrt{2D}\int_0^t \vec{\zeta}(t'')(1-e^{\frac{\gamma}{m}(t''-t)})dt'' \right|^2 \right\rangle \tag{2.18}$$

This squared term consists of three contributions: a deterministic term proportional to $\langle v(0)^2\rangle$, a stochastic term from the noise integral, and a cross-term between the deterministic and stochastic parts. Due to $\langle\vec{\zeta}(t)\rangle = \vec{0}$, the average of the cross-term vanishes. Thus, the MSD is the sum of the average of the squared deterministic part and the average of the squared stochastic part.

The deterministic contribution to the MSD, assuming $\langle v_i(0)v_j(0)\rangle = \delta_{ij}\langle v_i^2(0)\rangle$:

$$\left\langle \left| \vec{v}(0)\frac{m}{\gamma}(1-e^{-\frac{\gamma}{m}t}) \right|^2 \right\rangle = \sum_{i=1}^{d}\left(\frac{m}{\gamma}(1-e^{-\frac{\gamma}{m}t})\right)^2\langle v_i^2(0)\rangle$$

Using the equipartition theorem for the initial velocity $\langle v_i^2(0)\rangle = k_BT/m$, the Deterministic MSD contribution is as follows:

$$= d\frac{k_BT}{m}\frac{m^2}{\gamma^2}(1-e^{-\frac{\gamma}{m}t})^2 = d\frac{k_BTm}{\gamma^2}(1-e^{-\frac{\gamma}{m}t})^2 \tag{2.19}$$

This term is significant at short times but decays to zero as $t \to \infty$, reflecting the damping of the initial velocity.

The stochastic contribution to the MSD arises from the random force. Using the property of the noise, $\langle\zeta_i(t'')\zeta_j(t''')\rangle = \delta_{ij}\delta(t''-t''')$:

$$\begin{aligned}
&\left\langle \left| \frac{m}{\gamma}\sqrt{2D}\int_0^t \vec{\zeta}(t'')(1-e^{\frac{\gamma}{m}(t''-t)})dt'' \right|^2 \right\rangle \\
&= \left(\frac{m}{\gamma}\right)^2(2D)\sum_{i=1}^{d}\int_0^t\int_0^t \langle\zeta_i(t'')\zeta_i(t''')\rangle(1-e^{\frac{\gamma}{m}(t''-t)})(1-e^{\frac{\gamma}{m}(t'''-t)})dt''dt''' \\
&= 2Dd\frac{m^2}{\gamma^2}\int_0^t(1-e^{\frac{\gamma}{m}(t'-t)})^2dt'
\end{aligned}$$

Evaluating the integral:

$$\begin{aligned}\int_0^t (1 - e^{\frac{\gamma}{m}(t'-t)})^2 dt' &= \int_0^t (1 - 2e^{\frac{\gamma}{m}(t'-t)} + e^{\frac{2\gamma}{m}(t'-t)}) dt' \\ &= \left[t' - 2\frac{m}{\gamma} e^{\frac{\gamma}{m}(t'-t)} + \frac{m}{2\gamma} e^{\frac{2\gamma}{m}(t'-t)} \right]_0^t \\ &= t - 2\frac{m}{\gamma}(1 - e^{-\frac{\gamma}{m}t}) + \frac{m}{2\gamma}(1 - e^{-\frac{2\gamma}{m}t})\end{aligned}$$

Substituting this back and using $D = k_B T\gamma/m^2$, the stochastic MSD contribution is as follows:

$$= 2d\frac{k_B T}{\gamma}\left[t - \frac{2m}{\gamma}(1 - e^{-\frac{\gamma}{m}t}) + \frac{m}{2\gamma}(1 - e^{-\frac{2\gamma}{m}t}) \right] \tag{2.20}$$

Finally, summing the deterministic (Eq. 2.19) and stochastic (Eq. 2.20) contributions to obtain the full MSD:

$$\langle |\vec{r}(t) - \vec{r}(0)|^2 \rangle = 2d\frac{k_B T}{\gamma}\left[t - \frac{m}{\gamma}(1 - e^{-\frac{\gamma}{m}t}) \right] \tag{2.21}$$

This general expression for the MSD of an underdamped Brownian particle reveals two distinct regimes:

- **Short-time ballistic regime ($t \ll m/\gamma$):** In this regime, the particle's inertia dominates over friction. Expanding the exponential term $e^{-x} \approx 1 - x + x^2/2$ for small $x = \gamma t/m$:

  $$1 - e^{-\frac{\gamma}{m}t} \approx \frac{\gamma}{m}t - \frac{1}{2}\left(\frac{\gamma}{m}t\right)^2$$

  Substituting this into Eq. (2.21):

  $$\begin{aligned}\langle |\vec{r}(t) - \vec{r}(0)|^2 \rangle \approx& 2d\frac{k_B T}{\gamma}\left[t - \frac{m}{\gamma}\left(\frac{\gamma}{m}t - \frac{1}{2}\left(\frac{\gamma}{m}t\right)^2 \right) \right] \\ \approx& 2d\frac{k_B T}{\gamma}\left[t - t + \frac{m}{2\gamma}\left(\frac{\gamma}{m}t\right)^2 \right] \\ \approx& 2d\frac{k_B T}{\gamma}\left[\frac{\gamma^2}{2m\gamma}t^2 \right] = d\frac{k_B T}{m}t^2\end{aligned}$$

  $$\langle |\vec{r}(t) - \vec{r}(0)|^2 \rangle \approx d\frac{k_B T}{m}t^2 \tag{2.22}$$

  This quadratic dependence on time, characteristic of ballistic motion, indi-

cates that the particle's initial velocity (or velocity acquired from short-lived thermal kicks) largely dictates its displacement before viscous drag significantly slows it down.

- **Long-time diffusive regime ($t \gg m/\gamma$):** In this regime, inertia becomes negligible compared to the viscous damping, and the exponential term $e^{-\frac{\gamma}{m}t}$ rapidly approaches zero. The MSD simplifies to:

$$\langle |\vec{r}(t) - \vec{r}(0)|^2 \rangle \approx 2d\frac{k_B T}{\gamma}t \tag{2.23}$$

This linear dependence on time is the hallmark of diffusive behavior, where the particle's displacement is dominated by random thermal kicks, leading to a random walk. The coefficient of t defines the diffusion coefficient. From this, we can define the translational diffusion coefficient D_T as:

$$D_T = \frac{k_B T}{\gamma} \tag{2.24}$$

Thus, for long times, the MSD is given by $\langle |\vec{r}(t) - \vec{r}(0)|^2 \rangle = 2dD_T t$. This result is a direct consequence of the Einstein-Smoluchowski relation and forms the basis of diffusion theory.

Overdamped Brownian Motion (Smoluchowski Equation)

In many physical systems, particularly at the micro- and nano-scales where viscous forces are dominant and inertia is negligible, the momentum relaxation time $\tau_m = m/\gamma$ is extremely short compared to typical experimental timescales. In such cases, the inertial term $m\frac{d\vec{v}}{dt}$ in the Langevin equation (Eq. 2.1) can be safely neglected, leading to the overdamped limit or low Reynolds number regime. In this regime, the velocity of the particle is essentially an instantaneous balance of the forces acting upon it. The Langevin equation simplifies to:

$$\vec{0} = -\gamma\vec{v} - \nabla U(\vec{r}) + \vec{F}(t) \tag{2.25}$$

Rearranging to solve for velocity:

$$\vec{v}(t) = \frac{d\vec{r}}{dt} = -\frac{1}{\gamma}\nabla U(\vec{r}) + \frac{1}{\gamma}\vec{F}(t) \tag{2.26}$$

Substituting the noise properties from Eq. (2.3) and the fluctuation-dissipation theorem $D_p = k_B T\gamma$:

$$\frac{d\vec{r}}{dt} = -\frac{1}{\gamma}\nabla U(\vec{r}) + \sqrt{2D}\vec{\zeta}(t) \tag{2.27}$$

where $\vec{\zeta}(t)$ is normalized Gaussian white noise.

In this limit, the position itself becomes the primary stochastic variable, and the ballistic regime of the MSD disappears. The MSD for an overdamped free Brownian particle ($\nabla U = \vec{0}$) immediately exhibits diffusive behavior:

$$\langle|\vec{r}(t) - \vec{r}(0)|^2\rangle = 2dD_T t = 2d\frac{k_B T}{\gamma}t \tag{2.28}$$

The overdamped limit is particularly relevant for modeling many biological and synthetic active systems, including the swimmers within an anisotropic environment in this dissertation, as they typically operate in low Reynolds number environments where viscous forces dominate.

Translational Diffusion

The fundamental characteristic of free Brownian motion is its translational diffusion, where the particle spreads out over time. This is quantified by the Mean Squared Displacement (MSD),

$$\langle\Delta r^2(t)\rangle = \langle|\vec{r}(t) - \vec{r}(0)|^2\rangle.$$

For a 2D passive Brownian particle, the MSD grows linearly with time:

$$\langle\Delta r^2(t)\rangle = 4D_T t.$$

Here, D_T is the translational diffusion coefficient.

Einstein's Diffusion Theory (1905) established a crucial relationship between this diffusion coefficient and the microscopic properties of the system. For a spherical particle of radius R in an isotropic fluid with viscosity ν at temperature T, the translational diffusion coefficient is given by the Stokes-Einstein relation:

$$D_T = \frac{k_B T}{6\pi\nu R}.$$

This relation highlights that thermal energy ($k_B T$) drives the diffusion, while the viscous drag ($\gamma = 6\pi\nu R$) opposes it. It is a direct consequence of the fluctuation-

dissipation theorem for translational motion.

Rotational Diffusion

In addition to translational motion, passive particles also undergo rotational diffusion, where their orientation randomly changes due to thermal kicks from the fluid. This is important for anisotropic particles or for coupling with active propulsion. For a spherical particle, its rotational diffusion is characterized by the rotational diffusion coefficient D_R, given by:

$$D_R = \frac{k_B T}{8\pi\nu R^3}. \tag{2.29}$$

The characteristic time scale for rotational decorrelation is $\tau_R = 1/D_R$. Note the stark difference in scaling with particle radius: $D_T \propto R^{-1}$ while $D_R \propto R^{-3}$. This means smaller particles reorient much faster than they translate, and vice-versa for larger particles.

For a 2D passive Brownian particle, the stochastic equations of motion (neglecting inertia) are:

$$\dot{x} = \sqrt{2D_T}\zeta_x(t) \tag{2.30}$$

$$\dot{y} = \sqrt{2D_T}\zeta_y(t) \tag{2.31}$$

$$\dot{\varphi} = \sqrt{2D_R}\eta(t) \tag{2.32}$$

where (x, y) is the particle's position, φ is its orientation (for an anisotropic particle or just a reference angle for a sphere), and $\zeta_x(t)$, $\zeta_y(t)$, and $\eta(t)$ are independent Gaussian white noise processes with zero mean and correlation $\langle \zeta_i(t)\zeta_j(t')\rangle = \delta_{ij}\delta(t - t')$. Importantly, for passive particles, the translational and rotational motions are generally decoupled in a homogeneous isotropic environment.

2.2.2 Active Brownian Motion (ABM)

Active Brownian Motion (ABM) describes the dynamics of self-propelled particles, where the particle itself continuously converts energy into directed motion, driving it out of equilibrium. The active force $\vec{f}_{\text{act}}$ is central to ABM. For the simplest model, the Active Brownian Particle (ABP), this force is of constant magnitude v_0 (the self-propulsion speed) and acts along the particle's internal orientation $\hat{u}(t)$.

In the overdamped limit, the Langevin equation for a free ABP (i.e., no external potential, $U(\vec{r}) = 0$) is:

$$\gamma \frac{d\vec{r}}{dt} = v_0 \hat{u}(t) + \sqrt{2D_T}\vec{\zeta}(t). \tag{2.33}$$

Equation (2.33) can be explicitly written in terms of spatial coordinates ((x, y) in 2D) and an orientation angle φ,

$$\dot{x} = v_0 \cos\varphi(t) + \sqrt{2D_T}\zeta_x(t) \tag{2.34}$$

$$\dot{y} = v_0 \sin\varphi(t) + \sqrt{2D_T}\zeta_y(t) \tag{2.35}$$

$$\dot{\varphi} = \sqrt{2D_R}\eta(t) \tag{2.36}$$

Here, $\hat{u}(t) = (\cos\varphi(t), \sin\varphi(t))$ is the orientation vector. Unlike PBM, the translational motion is now coupled to the rotational motion through the self-propulsion term $v_0\hat{u}(t)$.

Persistence and Ballistic Motion

The constant self-propulsion v_0 means that active particles exhibit persistent motion over short to intermediate timescales. The particle continues to move in roughly the same direction until its orientation is changed by rotational diffusion. The characteristic length scale over which this directed motion persists is the persistence length L_p:

$$L_p = \frac{v_0}{D_R} = v_0\tau_R. \tag{2.37}$$

This length quantifies the average distance an active particle travels before its direction of motion significantly changes.

The average trajectory $\langle\vec{r}(t)\rangle$ of an ABP reveals this initial ballistic motion. Assuming an initial position $\vec{r}(0) = (0, 0)$ and orientation $\varphi(0) = 0$ (i.e., initially moving along the x-axis), the average position is:

$$\langle x(t)\rangle = \frac{v_0}{D_R}(1 - e^{-D_R t}) = v_0\tau_R(1 - e^{-t/\tau_R}) \tag{2.38}$$

$$\langle y(t)\rangle = 0. \tag{2.39}$$

At short times ($t \ll \tau_R$), $\langle x(t)\rangle \approx v_0 t$, indicating ballistic (directed) motion. At long times ($t \gg \tau_R$), $\langle x(t)\rangle \approx v_0\tau_R = L_p$, meaning the average directed motion saturates as the orientation becomes completely random.

Mean Squared Displacement (MSD) for ABM

The MSD for an active Brownian particle captures both its short-time ballistic behavior and its long-time enhanced diffusion. For a 2D free ABP, the MSD is given by:

$$\langle \Delta r^2(t) \rangle = 4D_T t + \frac{2v_0^2}{D_R^2}(D_R t - 1 + e^{-D_R t}). \tag{2.40}$$

Let's analyze its behavior:

- **Short times ($t \ll \tau_R = 1/D_R$):** From an expansion of the exponential term,

  $$e^{-D_R t} \approx 1 - D_R t + \frac{1}{2}(D_R t)^2,$$

  the MSD becomes

  $$\langle \Delta r^2(t) \rangle \approx 4D_T t + \frac{2v_0^2}{D_R^2}\left(D_R t - 1 + (1 - D_R t + \frac{1}{2}(D_R t)^2)\right) = 4D_T t + v_0^2 t^2.$$

  The $v_0^2 t^2$ term indicates ballistic (directed) motion, characteristic of active particles over short timescales. The $4D_T t$ term accounts for the underlying thermal diffusion.

- **Long times ($t \gg \tau_R = 1/D_R$):** As $e^{-D_R t} \to 0$, the MSD simplifies to:

  $$\langle \Delta r^2(t) \rangle \approx 4D_T t + \frac{2v_0^2}{D_R^2}(D_R t - 1) \approx 4D_T t + \frac{2v_0^2}{D_R} t = 4\left(D_T + \frac{v_0^2}{2D_R}\right) t.$$

  This linear growth with time indicates diffusive behavior, but with an enhanced effective diffusion coefficient:

  $$D_{eff} = D_T + \frac{v_0^2}{2D_R}. \tag{2.41}$$

  This shows that the persistent active motion contributes significantly to the long-time spreading of the particles.

2.2.3 Comparison of Passive and Active Brownian Motion in 2D

To fully appreciate the distinctions between passive and active Brownian motion, it is instructive to compare their behaviors for single spherical particles

of similar (hydrodynamic) radius R in a homogeneous environment, devoid of physical barriers or other particles.

Fundamental Differences in Dynamics

- **Energy Source and Equilibrium:** Passive Brownian particles are in thermal equilibrium with their environment, with their motion driven solely by thermal fluctuations. Active Brownian particles, however, are intrinsically out of equilibrium due to continuous energy consumption and conversion into self-propulsion.

- **Coupling of Degrees of Freedom:** For a passive Brownian particle in a homogeneous environment, the translational motion (described by x, y) and rotational motion (described by φ) are typically decoupled. Their stochastic equations of motion are given by the Eqs. (2.30), (2.31) and (2.32).

  In contrast, for a self-propelled active particle, the direction of motion is explicitly coupled to its orientation. The presence of the active propulsion velocity $v_0\vec{u}(t)$ links translation to rotation, leading to the coupled stochastic differential equations for ABM given by the Eqs. (2.34), (2.35) and (2.36).

Mean Squared Displacement (MSD) Comparison

The MSD serves as a direct quantitative measure to highlight their distinct behaviors:

- **PBM MSD:** For a passive Brownian particle in 2D, the MSD is purely diffusive at all times:

  $$\langle \Delta r^2(t) \rangle = 4D_T t,$$

  as shown in Figure 2.1 when $v = 0\ \mu\text{ms}^{-1}$.

  The average displacement $\langle x(t) \rangle$ and $\langle y(t) \rangle$ vanish due to the random, unbiased nature of thermal fluctuations.

- **ABM MSD:** For an active Brownian particle in 2D, the MSD exhibits a crossover from ballistic to enhanced diffusive behavior:

  $$\langle \Delta r^2(t) \rangle = 4D_T t + \frac{2v_0^2}{D_R^2}(D_R t - 1 + e^{-D_R t}).$$

At short times, the $v_0^2 t^2$ term dominates, representing persistent, directed motion (see Figure 2.1).

At long times ($t \gg \tau_R$), the motion becomes diffusive, but with an effective diffusion coefficient $D_{eff} = D_T + \frac{v_0^2}{2D_R}$, which is significantly larger than D_T due to the active component. The average trajectory $\langle x(t) \rangle = v_0 \tau_R (1 - e^{-t/\tau_R})$ shows this initial directed movement along the propulsion axis, reaching the persistence length $L_p = v_0 \tau_R$ at long times.

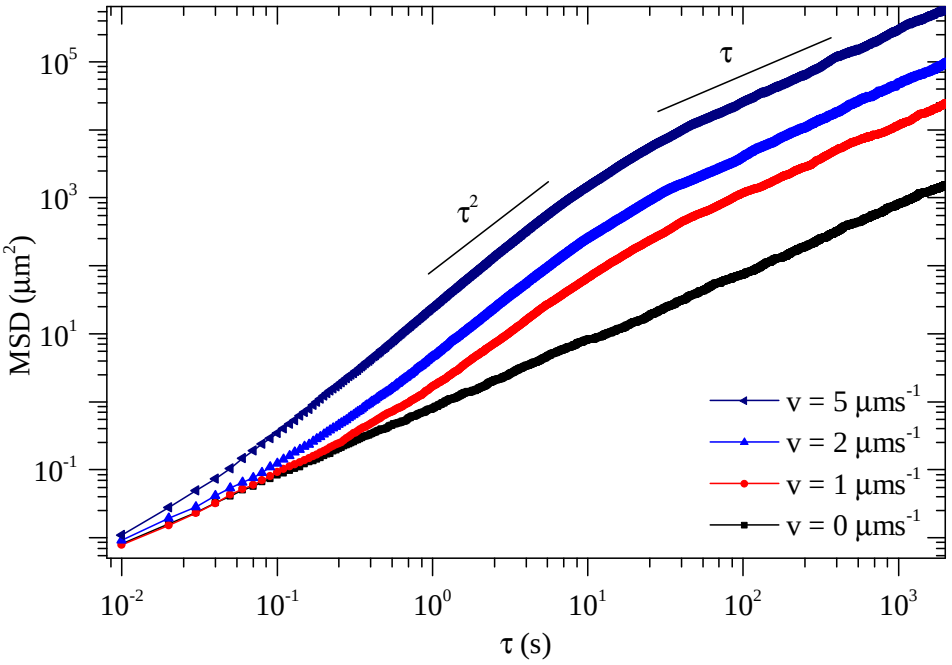

Figure 2.1: MSD in 2D for different velocities ($D_T = 0.2$ μm^{2}s^{-1}, $D_R = 0.17$ rad^{2}s^{-1} and $R \approx 0.1$ μm [3])

2.2.4 The Peclet Number

The relative importance of active, directed motion versus passive, diffusive spreading for an active Brownian particle is quantified by the dimensionless Péclet number (Pe). This number provides a crucial insight into the dominant transport mechanism in the system:

$$\mathrm{Pe} = \frac{v_0 L}{D}, \tag{2.42}$$

where v_0 is a characteristic speed, L is a characteristic length scale (e.g., particle size or persistence length), and D is a characteristic diffusion coefficient. For active

Brownian particles, a common definition is:

$$\mathrm{Pe} \propto \frac{v_0}{\sqrt{D_T D_R}}. \tag{2.43}$$

- If $\mathrm{Pe} \ll 1$: Diffusive motion dominates. The active propulsion is weak compared to thermal fluctuations, and the particle's behavior resembles that of a passive Brownian particle.
- If $\mathrm{Pe} \gg 1$: Directed (ballistic) motion prevails. The active propulsion is strong enough to overcome thermal random motion, leading to persistent, directed trajectories.

The Péclet number is a critical parameter in active matter, as it dictates whether a system's behavior will be primarily dictated by random thermal forces or by the directed activity of its constituents. Understanding its role is essential for predicting collective phenomena and designing active systems.

This model for active Brownian motion can be straightforwardly generalized to three dimensions, where particle position is described by (x, y, z) and orientation by polar and azimuthal angles that undergo Brownian motion on the unit sphere. The core principles of active versus passive behavior remain similar, adapted for the higher dimension.

Chapter 3

Liquid Crystals and Smectics

Before investigating the motion of active particles in complex anisotropic environments, here we introduce a few fundamental concepts in the area of liquid crystals, with emphasis on the smectic-A (SmA) phase and its characteristic Focal Conic Domains (FCDs). This discussion is based on classical and specialized literature [10, 9, 15, 5]. Furthermore, the specific director field data that characterizes the FCD patterns used in this work originate in the work by Liarte et al. [17].

3.1 Introduction

Most of us are familiar with typical states in condensed matter: solids, liquids, and gases. The main distinction between homogeneous, isotropic liquids, which have a uniform structure invariant by continuous rotations or translations, and crystalline solids, which retain their structure only under specific lattice translations and point group operations defined by the space group, lies in their order and symmetry. Liquids have short-range order but lack long-range order, exhibiting the highest possible symmetry. In contrast, crystalline solids display long-range positional and rotational order, with much lower symmetry than liquids. Between these extremes are materials that show short-range correlations in certain directions and long-range order in others, with symmetries that bridge the gap between those of liquids and crystals. One such intermediate order is orientational order. In a periodic crystal, specific directions are defined by vectors between neighboring particles at lattice sites. These directions are consistent throughout the lattice, leading to long-range orientational order, also known as bond-angle order. Remarkably, long-range orientational order can exist even without translational order [10, 9].

3.2 Isotropic and Nematic Phases

At sufficiently high temperatures, the anisotropic molecules that form liquid crystals are randomly oriented, and their centers of mass are randomly distributed, much like a conventional fluid. In this state, the system behaves as an isotropic fluid. Its structure factor is isotropic, typically displaying broad rings at wave numbers corresponding to the characteristic molecular dimensions (e.g., molecular length l and diameter a).

Upon cooling, or under specific external conditions, the isotropic liquid can undergo a phase transition to an ordered state. The first, and simplest, liquid crystalline phase to emerge for rod-like molecules is the nematic (N) phase. In the nematic phase, the elongated molecules spontaneously align, on average, parallel to a specific direction in space. This preferred direction is described by a unit vector called the director, denoted as $\hat{\mathbf{n}}$. Crucially, while the molecules exhibit long-range orientational order (they tend to point in the same direction), their centers of mass remain randomly distributed, akin to an isotropic fluid. This means the nematic phase breaks continuous rotational symmetry but preserves continuous translational invariance.

The nematic phase is invariant under rotations about an axis parallel to $\hat{\mathbf{n}}$, but not under rotations about axes perpendicular to $\hat{\mathbf{n}}$. It also possesses an inherent head-tail symmetry, meaning $\hat{\mathbf{n}}$ and $-\hat{\mathbf{n}}$ are physically indistinguishable (this defines a "non-polar" nematic). The degree of molecular alignment in the nematic phase is quantified by the scalar order parameter S:

$$S = \left\langle \frac{3}{2}\cos^2\theta - \frac{1}{2} \right\rangle, \tag{3.1}$$

where θ is the angle between the long axis of an individual molecule and the director $\hat{\mathbf{n}}$, and $\langle \dots \rangle$ denotes an ensemble average. For a perfectly isotropic state, $S = 0$, while for perfect alignment along the director, $S = 1$.

The transition from the isotropic to the nematic phase is largely driven by the anisotropic shape of the molecules and excluded volume interactions (anisotropic hard-core repulsion), as demonstrated by Onsager's seminal work in 1949. Aligning elongated molecules allows for a higher packing density, effectively increasing the entropy of the aligned state by allowing more translational freedom. The structure factor of the nematic phase reflects this broken rotational symmetry: it is axially symmetric perpendicular to $\hat{\mathbf{n}}$ but exhibits only two-fold symmetry

in planes containing $\hat{\mathbf{n}}$, often showing diffuse scattering concentrated along the director for molecular length scales.

3.3 Smectic Phases: Layered Order

As temperature is further reduced from the nematic phase, many liquid crystalline materials undergo another phase transition, leading to the formation of smectic liquid crystals. The defining characteristic of smectic phases is the development of one-dimensional positional order — molecules spontaneously arrange themselves into distinct, well-defined layers. Within these layers, the molecules typically retain liquid-like fluidity, allowing for relatively free movement in two dimensions, but exhibit a strong positional correlation perpendicular to the layers.

The most common smectic phase is the smectic-A (SmA) liquid crystal. In SmA, molecules are oriented, on average, perpendicular to the smectic layers, with their long axes parallel to the layer normal as shown in Figure 3.1. The introduction of this layering implies a periodic modulation of the molecular mass density in one direction. This can be described as a sinusoidal variation of the average molecular number-density, $\langle n(\vec{r})\rangle$:

$$\langle n(\vec{r})\rangle = n_0 + 2n_{q_0}\cos(q_0 z), \tag{3.2}$$

where n_0 is the average number density, n_{q_0} is the amplitude of the density modulation, and z is the coordinate along the layer normal. The wave vector $q_0 = 2\pi/d$ defines the periodicity of the layers, where d is the equilibrium layer spacing, typically of the order of the molecular length.

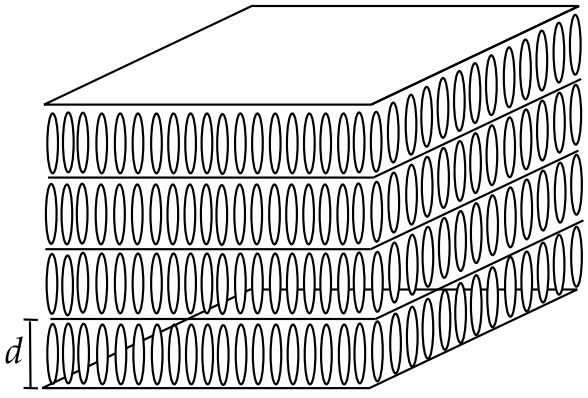

Figure 3.1: The arrangement of the layers in a Smectic-A liquid crystal

The presence of this mass density wave manifests in the static structure factor $S(\vec{q})$, which is the Fourier transform of the density-density correlation function. If the layering were perfectly long-ranged (like a true crystal), $S(\vec{q})$ would exhibit sharp Bragg peaks at $\vec{q} = \pm q_0 \hat{\mathbf{e}}_z$. However, due to thermal fluctuations, the ideal long-range periodic order of the smectic phase is subtly modified. As first predicted by Landau and Peierls and later formalized by the Mermin-Wagner theorem (in 2D systems, although its implications extend to 3D smectics), true long-range translational order is destroyed by thermal fluctuations at any finite temperature. Instead, smectics exhibit quasi-long-range order (QLRO), meaning correlations decay as a power law rather than exponentially. This leads to power-law singularities rather than true delta-function spikes in $S(\vec{q})$ at $\vec{q} = \pm q_0 \hat{\mathbf{e}}_z$, often referred to as quasi-Bragg peaks. The experimental observation of only two such peaks (at $\pm q_0$) in most thermotropic smectics confirms that a single sinusoidal modulation (Eq. 3.2) is an excellent representation of the density profile.

3.3.1 The Elastic Free Energy of Smectic-A Liquid Crystals

A crucial aspect for understanding the interaction of active particles with smectic liquid crystals is their elastic response to deformations. While liquids resist compression and shear, and crystalline solids resist all forms of deformation, smectics possess a unique elasticity that combines liquid-like fluidity within layers with solid-like resistance to layer distortions. Our focus on the SmA phase, and its interaction with active particles, requires an understanding of the energy cost associated with deforming its layered structure. This elastic energy will play a role in how active forces deform the smectic and how these deformations, in turn, influence particle motion.

Ideal smectic-A liquid crystals can be visualized as stacks of parallel, equally spaced planes, where molecules are aligned perpendicular to these planes (see Figure 3.1). These planes can be defined via the phase of the mass-density wave $\rho(\vec{r})$, which can be generally expanded in a Fourier series with period d:

$$\rho(\vec{r}) = \rho_0 + \rho_1 \cos \vec{q}_0 \cdot (\vec{r} - \vec{u}) + ... \tag{3.3}$$

$$= \rho_0 + \sum_{n \neq 0} [\rho_n e^{-in\vec{q}_0 \cdot \vec{u}} e^{in\vec{q}_0 \cdot \vec{r}} + \text{c.c.}]. \tag{3.4}$$

Where the wave vector $\vec{q}_0 = (2\pi/d)\hat{\mathbf{n}}_0 = (2\pi/d)\hat{\mathbf{e}}_z$ for layers parallel to the xy-plane, and $\langle \psi_n \rangle = \rho_n e^{-in\vec{q}_0 \cdot \vec{u}}$ are the complex amplitudes of the density mod-

ulation. As noted, for many smectics, the fundamental harmonic ($n = 1$) is dominant, simplifying the expression to:

$$\rho(\vec{r}) \approx \rho_0 + \rho_1 e^{-iq_0 u} e^{i\vec{q}_0 \cdot \vec{r}} + \text{c.c.}. \tag{3.5}$$

The complex amplitude $\rho_1 e^{-iq_0 u}$ acts as the primary order parameter for the SmA phase, differentiating it from the nematic phase. It can be written as:

$$\langle \psi_1 \rangle = \rho_1 e^{-iq_0 u}, \tag{3.6}$$

where ρ_1 is the amplitude of the density wave. The planes have constant phase of the mass-density wave at wave number $\vec{q}_0$:

$$\phi \equiv \vec{q}_0 \cdot \vec{r} - q_0 u = 2\pi n, \quad n = 0, \pm 1, \pm 2, ... \tag{3.7}$$

When u is independent of $\vec{r}$:

$$\frac{2\pi}{d}(\hat{e}_z \cdot \vec{r}) - \frac{2\pi}{d} u = -2\pi n,$$

defines the set uniformly spaced planes $z - u = nd$ perpendicular to the z-axis.

A distortion of the smectic layers, see Figure 3.2, can be represented by a spatially varying phase $\phi_1(\vec{r})$. If we define a layer displacement field $u(\vec{r})$ such that the actual position of a layer, originally at $z = nd$, is now at $z = nd + u(\vec{r})$, then the phase can be written as $\phi_1(\vec{r}) = q_0 z - q_0 u(\vec{r})$. The planes of constant phase correspond to $\vec{q}_0 \cdot \vec{r} - q_0 u(\vec{r}) = \text{constant}$.

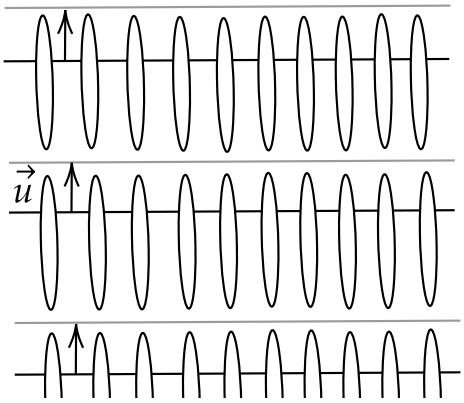

Figure 3.2: Constant displacement of the layer by $\vec{u}$

Alternatively, uniform translation $\vec{r}^{\alpha} \rightarrow \vec{r}^{\alpha} + u\hat{e}_z$, of all the molecules of the

smectic a distance u along the z-axis:

$$\begin{aligned}\langle\psi_n\rangle =& \frac{1}{V}\int d^3x e^{-in\vec{q}_0\cdot\vec{r}}\langle\psi_n(\vec{r})\rangle \qquad (3.8)\\ =& \frac{1}{V}\int d^3x e^{-in\vec{q}_0\cdot\vec{r}}\langle\sum_\alpha \delta(\vec{r}-\vec{r}^\alpha)\rangle\\ =& \frac{1}{V}\langle\sum_\alpha\int d^3x e^{-in\vec{q}_0\cdot\vec{r}}\delta(\vec{r}-\vec{r}^\alpha)\rangle\\ =& \frac{1}{V}\langle\sum_\alpha e^{-in\vec{q}_0\cdot\vec{r}^\alpha}\rangle \qquad (3.9)\end{aligned}$$

Translation $\vec{r}^\alpha \to \vec{r}^\alpha + u\hat{e}_z$:

$$\begin{aligned}\langle\psi_n'\rangle =& \frac{1}{V}\langle\sum_\alpha e^{-in\vec{q}_0\cdot(\vec{r}^\alpha+u\hat{e}_z)}\rangle\\ =& \frac{1}{V}\sum_\alpha\langle e^{-in\vec{q}_0\cdot\vec{r}^\alpha}e^{-in\vec{q}_0\cdot u\hat{e}_z}\rangle\\ =& \frac{1}{V}\sum_\alpha\langle e^{-in\vec{q}_0\cdot\vec{r}^\alpha}\rangle e^{-inq_0u}\\ =& \langle\psi_n\rangle e^{-inq_0u} \qquad (3.10)\end{aligned}$$

The phase ϕ_n decrease by nq_0u: $\phi_n = \phi_n^0 - nq_0u$ where ϕ_n^0 is the phase when $u = 0$.

The unit normal to the layers $\hat{N}(\vec{r})$ is given by the normalized gradient of the phase $\phi(\vec{r}) = q_0z - q_0u(\vec{r})$:

$$\hat{N}(\vec{r}) = \frac{\nabla\phi}{|\nabla\phi|} = \frac{(-q_0\nabla_x u, -q_0\nabla_y u, q_0)}{q_0\sqrt{1+(\nabla_\perp u)^2}} \approx (-\nabla_x u, -\nabla_y u, 1) + O[(\nabla u)^2]. \quad (3.11)$$

In the SmA phase, the average molecular orientation (the director $\hat{\mathbf{n}}$) is parallel to the layer normal $\hat{N}$.

The elastic free energy for smectic liquid crystals accounts for the energy cost associated with deforming these layers from their ideal, flat configuration. The leading-order elastic free energy density for a SmA liquid crystal, considering only deformations of the layer displacement $u(\vec{r})$, is given by:

$$F_{el} = \frac{1}{2}\int d^3x\left[B\left(\frac{\partial u}{\partial z}\right)^2 + K_1(\nabla_\perp^2 u)^2\right]. \qquad (3.12)$$

Let's explain each term:

- $B\left(\frac{\partial u}{\partial z}\right)^2$: This term quantifies the energy cost associated with layer compression or stretching. $\frac{\partial u}{\partial z}$ represents the local change in layer spacing along the layer normal (z-axis). If $\frac{\partial u}{\partial z} > 0$, the layers are compressed; if $\frac{\partial u}{\partial z} < 0$, they are stretched. B is the bulk modulus of layer compression, a macroscopic elastic constant unique to smectics, representing their solid-like resistance to changes in layer spacing. This term describes the energy stored in a smectic configuration where layers are locally stretched or compressed.

- $K_1(\nabla_\perp^2 u)^2$: This term quantifies the energy cost associated with layer bending (director splay distortion). The quantity $\nabla_\perp^2 u$ (where $\nabla_\perp^2 = \frac{\partial^2}{\partial x^2} + \frac{\partial^2}{\partial y^2}$) describes the local curvature of the layers in the plane perpendicular to the layer normal. For small distortions, $\nabla_\perp^2 u$ is approximately the divergence of the layer normal, $\nabla \cdot \hat{N}$. K_1 is the splay elastic constant, inherited from the Frank elastic theory for nematics, and it represents the energy cost of bending the layers. The inverse of $\nabla_\perp^2 u$ is related to the radius of curvature of the bent layer.

It is important to note that this elastic energy neglects higher-order derivatives like $(\nabla_{||}^2 u)(\nabla_\perp^2 u)$ or $(\nabla_{||}^2 u)^2$, as they are typically much smaller contributions at long wavelengths. This free energy provides the fundamental description of low-energy deformations in SmA liquid crystals.

This form of smectic elastic energy can also be understood by considering the coupling between the layer displacement field u and the nematic director $\hat{\mathbf{n}}$ (which aligns with the layer normal $\hat{N}$ in SmA). Whereas there is no energy cost associated with a joint rigid rotation of layers and molecules, there is an energy cost if the molecules deviate from aligning normal to the local layers. This leads to a more general free energy:

$$F_{el} = \frac{1}{2}\int d^3x \left[B\left(\frac{\partial u}{\partial z}\right)^2 + D(\nabla_\perp u + \delta\hat{\mathbf{n}})^2\right] + F_{\text{Frank}}(\hat{\mathbf{n}}), \tag{3.13}$$

where $\delta\hat{\mathbf{n}}$ is the deviation of the director from the ideal $\hat{\mathbf{e}}_z$ and $F_{\text{Frank}}(\hat{\mathbf{n}})$ is the Frank elastic energy for the nematic director given as:

$$F_{\text{Frank}}(\hat{\mathbf{n}}) = \frac{1}{2}\int d^3x[K_1(\nabla\cdot\hat{\mathbf{n}})^2 + K_2(\hat{\mathbf{n}}\cdot(\nabla\times\hat{\mathbf{n}}))^2 + K_3(\hat{\mathbf{n}}\times(\nabla\times\hat{\mathbf{n}}))^2], \tag{3.14}$$

where K_1, K_2 and K_3 account the splay, twist, and bend distortion, respectively as shown in Figure 3.3. The term $D(\nabla_\perp u + \delta\hat{\mathbf{n}})^2$ forces the director to align with

the local layer normal. Minimizing this free energy with respect to $\delta\hat{\mathbf{n}}$ shows that $\delta\hat{\mathbf{n}} = -\nabla_\perp u$. Substituting this back into the equation, and recognizing that $\nabla_\perp^2 u$ corresponds to splay distortions of the director, one recovers Eq. (3.12).

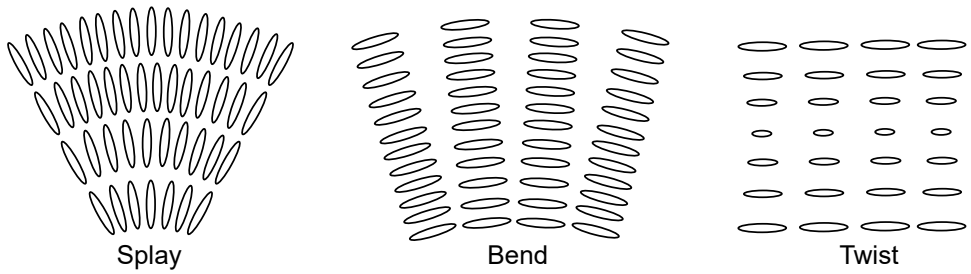

Figure 3.3: Splay, bend and twist distortions in SmA liquid crystal.

This coupled description further reveals that twist (K_2) and bend (K_3) distortions of the director are "expelled" from the smectic-A phase at long wavelengths. This means they are energetically very costly compared to splay, leading to short penetration depths $\lambda_2 = (K_2/D)^{1/2}$ and $\lambda_3 = (K_3/D)^{1/2}$. Thus, while both translational and rotational degrees of freedom exist, the low-energy elastic distortions in SmA are primarily described by the single translational elastic variable $u(\vec{r})$, which effectively dictates the local splay of the director and the bending of the layers.

3.4 Focal Conic Domains (FCDs)

Focal Conic Domains (FCDs) are fundamental architectural elements of smectic liquid crystals, representing ubiquitous patterns of layer deformation that minimize (or locally minimize) the smectic elastic free energy under certain conditions. They are crucial for understanding the macroscopic behavior of smectics, especially in confined geometries or under external fields. In the context of this thesis, FCDs are particularly important as they define the complex anisotropic environment within which the active Brownian particles (ABPs) will navigate. The director field associated with these FCDs provides the spatially varying orientational landscape that influences the ABPs' alignment and, consequently, their trajectories and transport properties.

The concept of FCDs emerged from early observations of smectic textures under polarizing microscopes. As early as the late 19th and early 20th centuries, pioneering work by Georges Friedel and others described characteristic patterns

of ellipses and hyperbolas that appeared when smectic phases formed (Figure 3.4). Friedel recognized these patterns as macroscopic manifestations of specific arrangements of the smectic layers, which, despite being fluid in two dimensions, exhibited a remarkable tendency to maintain constant interlayer spacing.

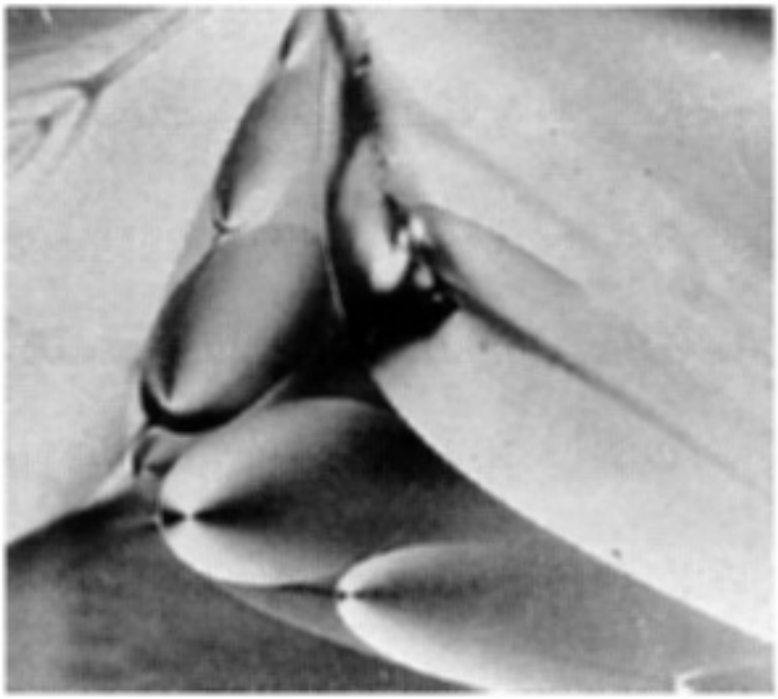

Figure 3.4: **Focal conic domains:** Pattern of ellipses and hyperbolas characteristic of the smectic-A microstructure. Image extracted from [10].

The rigorous theoretical framework for FCDs was later developed through an elegant geometric approach, largely attributed to the work of P. E. Cladis, M. Kleman, and ultimately synthesized by Pierre-Gilles de Gennes. This geometric theory revealed that the seemingly complex optical patterns were, in fact, projections of highly ordered, specific layer configurations resulting from the fundamental elastic properties of smectics. These configurations represented energetically favorable ways for the intrinsically layered smectic phase to accommodate curvature and respond to boundary conditions, forming defects that are topologically required or energetically preferred.

The geometric foundation of FCDs lies in a remarkable property of smectic-A layers: if they are to maintain a constant layer thickness everywhere, their normals must form a congruence of straight lines. This is a purely geometric constraint derived from the incompressibility of the smectic layers along their normal direction. If we consider a stack of smectic layers, any deformation that preserves constant

layer spacing implies that the distance along a normal between any two layers must remain constant. This is only possible if all the normals to these layers are straight lines, forming a family of straight lines in three-dimensional space.

Furthermore, for these straight normals to consistently be perpendicular to the family of parallel surfaces (the smectic layers), they must possess a unique geometric property: they must be simultaneously tangent to two surfaces, known as the focal surfaces. For a generic family of parallel surfaces, these focal surfaces are the envelopes of their normals. In the context of smectic liquid crystals, for deformations that preserve constant layer spacing, these focal surfaces degenerate into two distinct curves that are orthogonal conic sections, specifically an ellipse and a hyperbola, sharing common foci. This is the origin of the term "focal conic."

Each smectic layer within an FCD can be understood as a portion of a *Dupin cyclide*, a complex three-dimensional surface that is characterized by having its normals intersect two focal curves. The simplest FCDs are build on a singular circle with a straight line passing through its center; the so-called toroidal focal conics. The smectic layers are then arranged as a stack of concentric tori (doughnut-shaped surfaces) whose axes are aligned along the straight-line, and whose cross-sections are circles with centers on the focal circle (Fig. 3.5a). The most common FCD is of the elliptic-hyperbolic type — instead of a circle and straight line one sees a singular ellipse and a singular hyperbola so that the vertex of the hyperbola passes through one of the foci of the ellipse (Fig. 3.5b). This intricate geometry ensures that the layer spacing is constant throughout the domain.

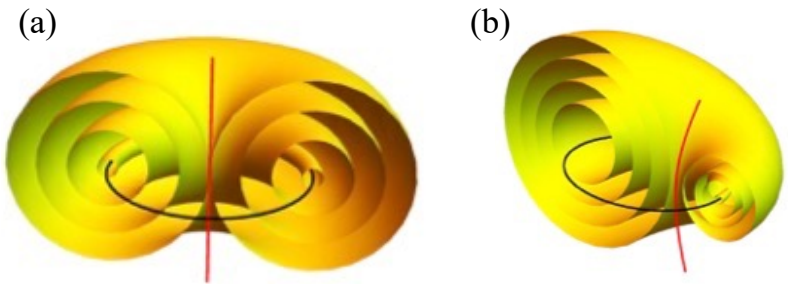

Figure 3.5: Toroidal (a) and elliptic-hyperbolic (b) types of focal conic domains.

3.5 Simulations: Smectic Microstructure

To provide the detailed background for the SmA environment that will be used in our active-particle simulations, we will consider the director fields obtained

from numerical simulations of a smectic-A liquid crystal based on the work by Liarte et al. (2015) [17]. Here we describe their model, in which a smectic texture filled with FCDs spontaneously emerge from random initial configurations, by means of an elastic free energy minimization.

3.5.1 Modeling Smectic-A Dynamics and FCD Generation

The study by Liarte et al. (2015) employs a continuum elastic model to simulate the dynamics and formation of FCDs in smectic-A liquid crystals. Their approach starts from a generalized elastic free energy functional, Ψ, which governs the behavior of the smectic layer normal field $\hat{\mathbf{N}}$.

Elastic Free Energy Functional

The system's total free energy, Ψ, is expressed as an integral over the spatial domain, incorporating contributions from the layer normal field $\hat{\mathbf{N}}$ and its derivatives:

$$\Psi = \int d\mathbf{r} \left[F(\hat{\mathbf{N}}, \partial_\mu \hat{\mathbf{N}}) + \vec{\lambda} \cdot (\nabla \times \hat{\mathbf{N}}) \right]. \tag{3.15}$$

Let's analyze the components of this functional:

- $F(\hat{\mathbf{N}}, \partial_\mu \hat{\mathbf{N}})$: This represents the free-energy density, a local contribution to the total energy that depends on the layer normal field $\hat{\mathbf{N}}$ itself and its spatial derivatives. In this model, $\hat{\mathbf{N}}$ is a continuous vector field whose magnitude $N = |\hat{\mathbf{N}}|$ can vary, especially near singularities.
- $\vec{\lambda} \cdot (\nabla \times \hat{\mathbf{N}})$: This term incorporates a Lagrange multiplier $\vec{\lambda}$ to enforce the constraint that the layer normal field must be curl-free ($\nabla \times \hat{\mathbf{N}} = 0$) in regions free of dislocations. The quantity $\nabla \times \hat{\mathbf{N}}$ represents the density of dislocations.

The free-energy density F is specifically formulated to capture the essential elastic properties of smectic-A liquid crystals, including deviations from ideal layer spacing and curvature:

$$F = \frac{B}{4}(1 - N^4)^2 + KN^2(\nabla \cdot \hat{\mathbf{N}})^2 + \frac{1}{4}K_{24}N^2 \nabla \cdot [(\hat{\mathbf{N}} \cdot \nabla)\hat{\mathbf{N}} - \hat{\mathbf{N}}(\nabla \cdot \hat{\mathbf{N}})]. \tag{3.16}$$

Let's explain each term:

- $\frac{B}{4}(1-N^4)^2$: This is the compression/extension term. It penalizes deviations of the magnitude of the layer normal field N from its ideal value of 1. B is the bulk modulus of layer compression, similar to the B constant in the simpler SmA elastic theory. The use of N^4 (instead of N^2) is motivated by connections to the tensorial order parameter in a more general Landau-de Gennes theory, reflecting that the lowest-order invariant term for nematic uniaxial order ($\mathrm{tr}(\mathbf{Q}^2)$) is proportional to N^4. This term describes the energy cost when smectic layers are stretched or compressed.

- $KN^2(\nabla\cdot\hat{\mathbf{N}})^2$: This term accounts for splay distortions of the layers. $\nabla\cdot\hat{\mathbf{N}}$ represents the divergence of the layer normal field, which quantifies how much the normals spread out or converge. This is directly related to the bending of smectic layers. K is the splay elastic constant. The N^2 pre-factor is used to stabilize line singularities by allowing a cutoff of the free energy near the focal lines.

- $\frac{1}{4}K_{24}N^2\nabla\cdot[(\hat{\mathbf{N}}\cdot\nabla)\hat{\mathbf{N}}-\hat{\mathbf{N}}(\nabla\cdot\hat{\mathbf{N}})]$: This is the saddle-splay (or Gaussian curvature) term. Except for the N^2 dependence of K_{24}, this is a total divergence term, which becomes a surface term that do not contribute to the bulk energy for systems with periodic boundary conditions. This term is associated with the Gaussian curvature of the smectic layers, and plays a role in the morphology of certain FCDs. K_{24} is the saddle-splay elastic constant, which is multiplied by N^2 here, for the reasons as K.

This free energy represents a comprehensive continuum model for the SmA phase, allowing for variations in both the orientation and the magnitude of the layer normal field, particularly important for describing highly distorted regions of FCDs.

Dynamical Equations: Gradient-Descent Evolution

To simulate the formation and evolution of FCDs, Liarte et al. (2015) model the dynamics of the layer normal field $\hat{\mathbf{N}}$ as a gradient-descent process. This approach assumes that $\hat{\mathbf{N}}$ continuously relaxes towards an equilibrium configuration that minimizes the free energy Ψ. The resulting partial differential equation for the evolution of $\hat{\mathbf{N}}$ is:

$$\gamma\dot{\hat{\mathbf{N}}} = -\left(\frac{\delta\Psi}{\delta\hat{\mathbf{N}}} - \left\langle\frac{\delta\Psi}{\delta\hat{\mathbf{N}}}\right\rangle\right). \tag{3.17}$$

Let's clarify the terms:

- $\gamma\dot{\hat{\mathbf{N}}}$: This represents the rate of change of the layer normal field, scaled by a rotational viscosity constant γ. This term drives the relaxation.
- $-\frac{\delta\Psi}{\delta\hat{\mathbf{N}}}$: This is the variational derivative (or functional derivative) of the free energy with respect to $\hat{\mathbf{N}}$. It represents the "force" that drives the field towards an energy minimum.
- $-\left\langle\frac{\delta\Psi}{\delta\hat{\mathbf{N}}}\right\rangle$: The spatial average of the variational derivative is subtracted. This term ensures the conservation of the overall number of layers within the simulated volume, preventing global changes in layer density during the relaxation process.

This gradient descent dynamics allows initially random configurations of the layer normal field to evolve into stable, low-energy FCD patterns. This dynamical model allows for the generation of various FCD structures from random initial conditions under specified boundary constraints. The numerical methods often involve spatial derivatives via Fourier transforms (FFTs) and time integration via schemes like Euler's method with adaptive step sizes. Boundary conditions (e.g., homeotropic or planar anchoring) are enforced to guide the formation of specific FCD types. These conditions dictate how the smectic layers or the director field interact with the confining surfaces. The authors employed homeotropic anchoring (layers parallel to the boundaries) and planar anchoring (layers perpendicular to the boundaries), often by mirroring the simulation volume or using specific constraints. This setup allows the system to relax into stable FCD patterns that minimize the free energy given the imposed constraints. The simulations begin from normally distributed random initial grids for the layer-normal field, which are then smoothed and subjected to these anchoring constraints. In Figure 3.6 shows simulated FCDs when planar anchoring is imposed.

The methodology presented by Liarte et al. (2015) for simulating FCDs is directly relevant for our simulations of active particles, as it provides the theoretical and computational basis for the static smectic environment in which our active Brownian particles will be studied.

In our work, we use the previously computed director fields ($\hat{\mathbf{n}}(\vec{r})$) obtained as the output of such FCD simulations. This means that the complex, spatially varying layered structure, including the characteristic patterns of ellipses and hyperbolas, is fixed in time within our simulation domain. The active Brownian particles (ABPs) then move within this given anisotropic landscape.

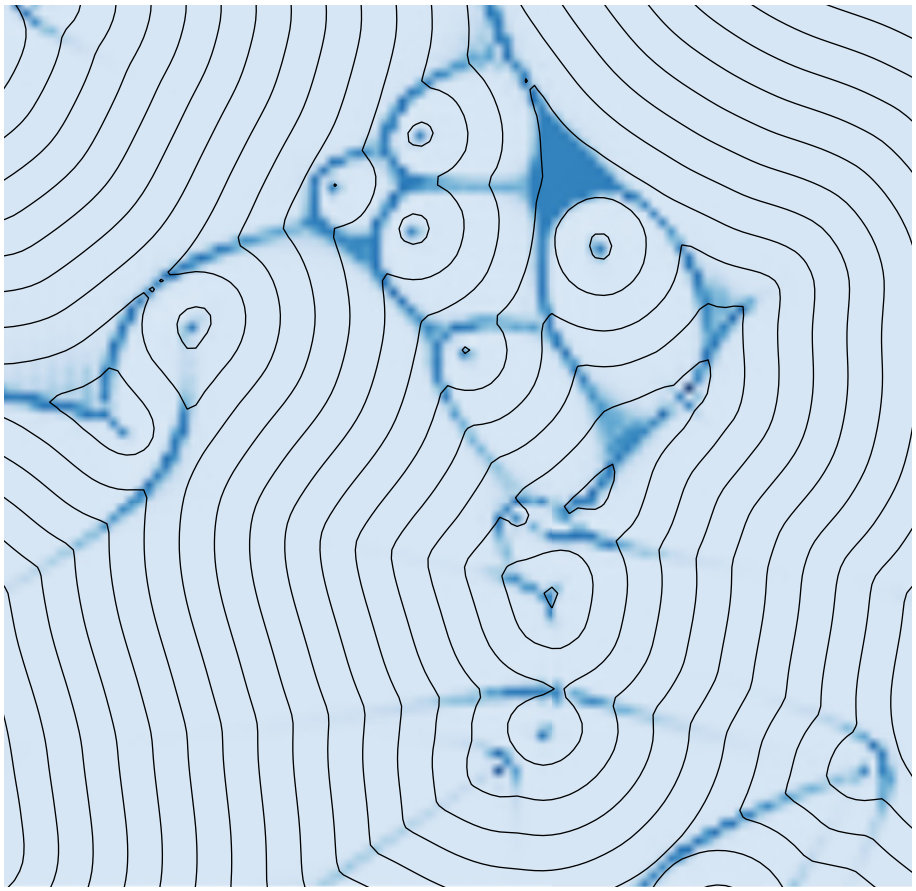

Figure 3.6: Simulated FCDs with planar anchoring (Extracted from [17]).

It is important to emphasize that, in our study, the active particles do not induce deformations or dynamics in the smectic phase. The elastic free energy of the smectic (Eq. (3.15)) thus describes the energy content of the FCD configuration itself, reflecting the inherent elastic cost of the spatial variations in the director field. This approach allows us to isolate and systematically study the impact of specific, complex smectic textures on active particle transport without the added complexity of a dynamically evolving smectic medium. By fixing the smectic configuration, we can precisely investigate how the spatial variations in layer curvature and director orientation, characteristic of FCDs, modulate the trajectories, diffusion, and overall transport properties of active particles.

Chapter 4

Results and Analysis

This chapter serves as the core of our numerical investigation, translating the theoretical framework of ABPs and smectic-A (SmA) liquid crystals with FCDs into a computational model. We begin by detailing the formulation of our specific model for ABPs interacting with a static SmA environment, explicitly explaining the inherent complexities that render an analytical solution for quantities like the Mean Squared Displacement (MSD) intractable, thus justifying our numerical approach. Subsequently, we describe the numerical simulation methodology employed, including the chosen integration algorithms, the definition of key parameters, and the process of incorporating the fixed smectic configurations into our simulations. The inspiration for our theoretical approach to active particles in liquid crystalline media is significantly drawn from the work of Ferreiro-Córdova et al. [12], while the SmA configurations were obtained from the study by Liarte et al. [17]. Finally, this chapter presents and thoroughly analyzes the results derived from these simulations, shedding light on the rich and often anomalous transport phenomena exhibited by ABPs in both flat and FCD-structured smectic environments.

4.1 Modeling Active Particle Dynamics

We investigate the dynamics of a self-propelled particle embedded in an ordered smectic A phase. The swimmer moves autonomously through the medium, which remains in thermodynamic equilibrium and exhibits spatially varying orientational order described by the local director field $\hat{\mathbf{n}}(\vec{r})$. The swimmer is characterized by its position $\vec{r}_s(t)$ and an orientation unit vector $\hat{u}(t)$, which defines the direction of active propulsion.

4.1.1 Physical Aspects of our Model

At its core, this model describes an *active Brownian particle* (ABP) that not only propels itself but also actively interacts with its environment. The smectic A phase, with its ordered layers and the local director field $\hat{\mathbf{n}}(\vec{r})$ (perpendicular to the layers), provides a spatially structured background. This structure is particularly rich in Focal Conic Domains (FCDs), which introduce complex, curved director fields.

The system is assumed to be *overdamped*, as mentioned in Chapter 2, so that the swimmers motion is dominated by drag and stochastic forces. This is a *Markov process* — the future state depends only on its current position and orientation, not on its history. This is a common and powerful simplification for many microscopic active systems. Crucially, its interaction with the smectic is *local*: the swimmer aligns itself with the director field at its current location, reflecting short-ranged physical interactions like steric exclusion or elastic coupling with the liquid crystal molecules. The overall system is rotationally invariant; any directional preference emerges from the local symmetry breaking of the director field.

The swimmer's translational motion is governed by an overdamped Langevin equation,

$$\frac{d\vec{r}_s(t)}{dt} = v_s\hat{u}(t) + \vec{\zeta}(t), \tag{4.1}$$

where v_s is a constant self-propulsion speed and $\vec{\zeta}(t)$ is a zero-mean stochastic translational force accounting for environmental fluctuations and particle-medium interactions.

The swimmer's orientation $\hat{u}(t)$ evolves over time via alignment with the local director field, driven by the gradient descent of an alignment energy. Importantly, it also includes a stochastic rotational term, reflecting intrinsic reorientational fluctuations or active stochastic reorientations:

$$\dot{\hat{u}} = -\frac{\delta E}{\delta \hat{u}} + \vec{\eta}(t). \tag{4.2}$$

Here, $\vec{\eta}(t)$ represents a zero-mean stochastic torque or rotational noise.

The alignment energy E is given by:

$$E = -\frac{k}{2}(\hat{u}\cdot\hat{\mathbf{n}})^2, \tag{4.3}$$

where $k > 0$ is the alignment strength. This energy is minimized when $\hat{u}$ aligns or

anti-aligns with the local director, which is a key characteristic of smectic A phases where molecules can align in either direction along the layer normal. Notice that $\hat{\boldsymbol{n}} = \boldsymbol{N}/|\boldsymbol{N}|$ is the unit layer-normal field.

To ensure that the orientation vector remains normalized on the unit sphere ($|\hat{u}| = 1$), the deterministic angular dynamics (the $-\frac{\delta E}{\delta \hat{u}}$ part) follow:

$$\left(\frac{d\hat{u}}{dt}\right)_{\text{deterministic}} = k(\hat{u}\cdot\hat{\mathbf{n}})\left[\hat{\mathbf{n}} - (\hat{u}\cdot\hat{\mathbf{n}})\hat{u}\right]. \tag{4.4}$$

This specific form ensures $\hat{u}\cdot\left(\frac{d\hat{u}}{dt}\right)_{\text{deterministic}} = 0$, thus preserving the unit magnitude. When rotational noise is included, the full angular dynamics become:

$$\frac{d\hat{u}}{dt} = k(\hat{u}\cdot\hat{\mathbf{n}})\left[\hat{\mathbf{n}} - (\hat{u}\cdot\hat{\mathbf{n}})\hat{u}\right] + \vec{\eta}(t). \tag{4.5}$$

The rotational noise $\vec{\eta}(t)$ acts perpendicularly to $\hat{u}$ to preserve its unit length, similar to how translational noise $\vec{\zeta}(t)$ influences $\vec{r}_s(t)$. Specifically, $\vec{\eta}(t)\cdot\hat{u}(t) = 0$.

4.1.2 Formulation in 2D

Here we consider the case where the active particle is restricted to move in a two-dimensional planar section of the smectic simulation. The layer-normal field $\hat{\boldsymbol{n}}$ is in the plane and forms an angle ϕ with the x-axis ($\hat{\mathbf{n}} = (\cos\phi, \sin\phi)$). The orientation vector $\hat{u}(t)$ can be described by a single angle $\theta(t)$ in the plane, such that $\hat{u}(t) = (\cos\theta(t), \sin\theta(t))$ as shown in Figure 4.1. The alignment energy in this case simplifies to:

$$E = -\frac{k}{2}\cos^2\varphi(t), \tag{4.6}$$

where $\varphi(t) = \theta(t) - \phi(\vec{r}_s(t))$ is the instantaneous angle between the swimmer's heading and the local director.

The angular dynamics for $\theta(t)$ then follow:

$$\dot{\theta} = -\frac{dE}{d\varphi} + \eta(t) = -\frac{k}{2}\sin(2\varphi) + \eta(t), \tag{4.7}$$

where $\eta(t)$ is the scalar rotational noise in 2D. This equation corresponds to an overdamped rotation towards alignment with the director, perturbed by continuous stochastic reorientations. This expression can be seen as the 2D counterpart of Eq. (4.5) and naturally emerges when the motion is constrained to a plane.

The 2D formulation is especially useful in describing swimmer dynamics in

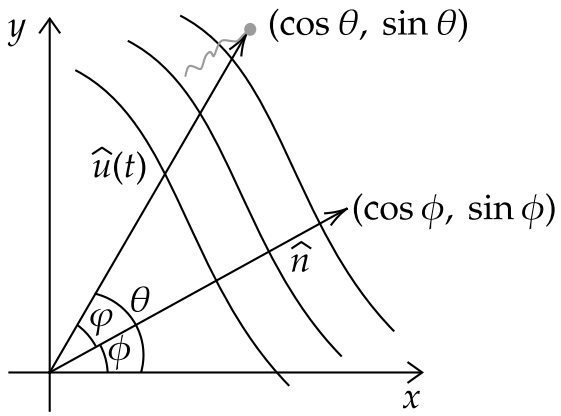

Figure 4.1: Particle direction and director field in 2D.

thin smectic films or within focal conic domains (FCDs) when the director field can vary, but is restricted to lie within the plane. The nonlinear nature of the angular relaxation term $\sin(2\varphi)$ reflects the symmetry of the underlying alignment energy and introduces anharmonic effects in the orientational dynamics. For small misalignment angles ($\varphi \approx 0$), the system behaves effectively harmonically ($\sin(2\varphi) \approx 2\varphi$), and the angular relaxation is approximately linear. This harmonic limit simplifies analytical treatment and mirrors the behavior of small fluctuations in the XY-model.

Therefore, our model captures both the geometric constraint of unit orientation and the complex interplay between local order, active motion, and stochastic reorientation, while respecting the symmetry and physical constraints imposed by the smectic microstructure.

4.1.3 Statistical Properties of Noise Terms:

To proceed with any theoretical or numerical analysis, it is crucial to define the statistical properties of the noise terms $\vec{\zeta}(t)$ and $\eta(t)$. Since we are considering a coarse-grained, effective theory, their properties must obey the following physical constraints:

- **Rotation invariance:** The system does not possess a global preferred direction. Therefore, all vectorial and rotational quantities must transform covariantly under global rotations.
- **Spatio-temporal locality:** The noises are assumed to be white in time and local in space. That is, $\vec{\zeta}(t)$ and $\eta(t)$ at a given time depend only on the local

properties at that time, and correlations at different times vanish.

- **Gaussian statistics:** On mesoscopic timescales, $\vec{\zeta}(t)$ and $\eta(t)$ can be considered the sum of many statistically independent microscopic fluctuations (e.g., collisions, kicks, thermal fluctuations), which, by the central limit theorem, implies that they follow Gaussian distributions.

Under these assumptions, the two-point correlations of the noises must be of the most general form consistent with these symmetries. Since the only vectorial quantity breaking isotropy locally is the smectic director field $\hat{\mathbf{n}}(\vec{r}_s)$, the two-point correlation function of the translational noise can include both isotropic and anisotropic components:

$$\langle \zeta_\alpha(t)\zeta_\beta(t')\rangle = 2D_T\delta_{\alpha\beta}\delta(t-t') + 2D_A n_\alpha(\vec{r}_s(t),t)n_\beta(\vec{r}_s(t),t)\delta(t-t'). \tag{4.8}$$

Here, D_T is the strength (diffusion coefficient) of the isotropic translational noise component (the same in all directions), and D_A quantifies the anisotropic translational contribution aligned along the local director. The delta function $\delta(t-t')$ ensures the temporal locality (white noise). The indices α, β run over the spatial dimensions (x, y in 2D; x, y, z in 3D).

For rotational noise, in 2D, it is a scalar quantity $\eta(t)$ whose correlation is given by:

$$\langle \eta(t)\eta(t')\rangle = 2D_R\delta(t-t'). \tag{4.9}$$

Here, D_R is the rotational diffusion coefficient, characterizing the strength of the angular fluctuations. In 3D, the rotational noise $\vec{\eta}(t)$ would be a vector perpendicular to $\hat{u}$, and its correlation would be more complex, typically involving projection operators to ensure perpendicularity:

$$\langle \eta_\alpha(t)\eta_\beta(t')\rangle = 2D_R(\delta_{\alpha\beta} - u_\alpha(t)u_\beta(t))\delta(t-t'). \tag{4.10}$$

Here we will focus on the 2D case, for which Eq. (4.9) is sufficient.

In addition, since the noise originates from interactions with the local microstructure, it is permissible in nonequilibrium systems for the noise to be correlated with the director field itself. Therefore, we include a possible cross-correlation term between translational noise and the director field:

$$\langle \zeta_\alpha(t)n_\beta(\vec{r}_s(t'),t')\rangle = 2D_{Tn}\,\delta_{\alpha\beta}\,\delta(t-t'), \tag{4.11}$$

where D_{Tn} is a phenomenological parameter measuring the correlation strength between the stochastic force and the local director. Importantly, we do *not* consider a cross-correlation between the rotational noise $\eta(t)$ and the director field $\hat{\mathbf{n}}$, as the rotational noise primarily stems from internal reorientational fluctuations or isotropic thermal torques rather than directly from anisotropic drag with the director field.

It is essential to emphasize that these parameters (D_T, D_A, D_R, and D_{Tn}) are *independent*, and are not constrained by any Einstein-type fluctuation-dissipation relation. This is because the swimmer is an active particle operating far from thermodynamic equilibrium. The noises are Gaussian and fully described by their means and covariances. Equations (4.8), (4.9), and (4.11) provide a complete statistical description of the fluctuations acting on the active particle in the smectic environment.

4.1.4 Mean motion of the ABP

We now analyze the average dynamics of the self-propelled particle governed by Eq. (4.1). Taking the ensemble average over realizations of the stochastic forces $\vec{\zeta}(t)$ and $\eta(t)$, and recalling that $\langle\vec{\zeta}(t)\rangle = 0$, we obtain an equation for the mean position of the swimmer:

$$\left\langle \frac{d\vec{r}_s(t)}{dt} \right\rangle = v_s\langle\hat{u}(t)\rangle. \tag{4.12}$$

The orientation $\hat{u}(t)$ evolves dynamically via relaxation toward the local director field $\hat{\mathbf{n}}(\vec{r}_s(t))$, according to Eq. (4.7) (in 2D), actively perturbed by rotational noise. Therefore, the mean direction of motion is determined by the average orientation of the swimmer, which is in turn influenced by the spatial structure of the smectic and the reorienting effect of the rotational noise.

The director field is not uniform but structured through the presence of FCDs, which impose strong spatial variation on $\hat{\mathbf{n}}(\vec{r})$. Consequently, the mean swimmer orientation $\langle\hat{u}(t)\rangle$ reflects an average over these deterministic textures, the alignment dynamics, and the randomizing effect of the rotational noise.

If the FCD texture is statistically isotropic over the region explored by the swimmer, then $\langle\hat{\mathbf{n}}\rangle = 0$, and the mean displacement remains zero over long times. However, if the texture is anisotropic, for example with a net alignment bias along the $\hat{\mathbf{z}}$-direction, then we can write:

$$\langle\vec{r}_s(t)\rangle = v_s t\langle\hat{u}\rangle \equiv v_z t\hat{\mathbf{z}}, \tag{4.13}$$

where $v_z = v_s|\langle\hat{u}\rangle|$ is the effective drift speed along the preferred direction of the domain.

Unlike models dominated solely by director fluctuations, here the rotational noise will actively work to reduce $\langle\hat{u}\rangle$ even in a uniform director field, leading to $\langle\hat{u}\rangle \to 0$ for large D_R. Thus, sustained ballistic transport for $\langle\vec{r}_s(t)\rangle$ only occurs if the alignment (k) and the director field provide a strong enough directional bias to overcome the stochastic effects of D_R.

4.1.5 Mean-Square Displacement of the ABP

To characterize the transport properties of the swimmer, we compute the mean-square displacement (MSD),

$$\langle\Delta\vec{r}_s^2(t)\rangle \equiv \left\langle [\vec{r}_s(t) - \vec{r}_s(0)]^2 \right\rangle. \tag{4.14}$$

From the equation of motion (4.1),

$$\frac{d\vec{r}_s(t)}{dt} = v_s\hat{u}(t) + \vec{\zeta}(t),$$

we can formally integrate the trajectory:

$$\vec{r}_s(t) = \vec{r}_s(0) + v_s\int_0^t \hat{u}(\tau)\,d\tau + \int_0^t \vec{\zeta}(\tau)d\tau. \tag{4.15}$$

The MSD is then given by:

$$\begin{aligned}\langle\Delta\vec{r}_s^2(t)\rangle = v_s^2\left\langle\left|\int_0^t \hat{u}(\tau)\,d\tau\right|^2\right\rangle + 2v_s\left\langle\left(\int_0^t \hat{u}(\tau)\,d\tau\right)\cdot\left(\int_0^t \vec{\zeta}(\tau')\,d\tau'\right)\right\rangle \\ + \left\langle\left|\int_0^t \vec{\zeta}(\tau)\,d\tau\right|^2\right\rangle.\end{aligned} \tag{4.16}$$

The noise-induced term in the MSD contributes:

$$\begin{aligned}\left\langle\left|\int_0^t \vec{\zeta}(\tau)\,d\tau\right|^2\right\rangle &= \int_0^t\int_0^t \langle\zeta_\alpha(\tau)\,\zeta_\beta(\tau')\rangle\,d\tau\,d\tau' \\ &= \int_0^t 2\left[D_T\delta_{\alpha\beta} + D_A\langle n_\alpha(\tau)n_\beta(\tau)\rangle\right]\,d\tau.\end{aligned} \tag{4.17}$$

Assuming isotropy or averaging over space within FCDs (i.e., assuming the

integral averages over many domains such that the average direction of $\hat{n}$ is random), we may write:

$$\langle n_\alpha n_\beta \rangle = \frac{1}{d}\delta_{\alpha\beta}, \tag{4.18}$$

in which case Eq. (4.17) simplifies to:

$$\left\langle \left| \int_0^t \vec{\zeta}(\tau)\, d\tau \right|^2 \right\rangle = 2d \left(D_T + \frac{D_A}{d} \right) t, \tag{4.19}$$

where d is the dimensionality (e.g., $d = 2$ or 3).

For the active term, we define the orientation autocorrelation:

$$C_u(\vec{r}_s(t) - \vec{r}_s(t+\tau), \tau) = \langle \hat{u}(\vec{r}_s(t), t)) \cdot \hat{u}(\vec{r}_s(t+\tau), t+\tau) \rangle, \tag{4.20}$$

redefined $\vec{r}_s(t) = \vec{r}'_s$ and $\vec{r}_s(t+\tau) = \vec{r}''_s$. Thus, leading to:

$$\begin{aligned} \left\langle \left| \int_0^t \hat{u}(\vec{r}'_s, t) \cdot \hat{u}(\vec{r}''_s, t+\tau) d\tau \right|^2 \right\rangle &= \int_0^t \int_0^t C_u(\vec{r}'_s - \vec{r}''_s, \tau' - \tau) d\tau\, d\tau' \\ &= 2\int_0^t (t-\tau) C_u(\vec{r}'_s - \vec{r}''_s, \tau)\, d\tau. \end{aligned} \tag{4.21}$$

Thus terms contributed to MSD:

$$\langle \Delta \vec{r}_s^2(t) \rangle = 2v_s^2 \int_0^t (t-\tau) C_u(\vec{r}'_s - \vec{r}''_s, \tau) d\tau + 2d \left(D_T + \frac{D_A}{d} \right) t. \tag{4.22}$$

The cross term in Eq. (4.16), $\left\langle \left(\int_0^t \hat{u}(\tau) d\tau \right) \cdot \left(\int_0^t \vec{\zeta}(\tau') d\tau' \right) \right\rangle$, also needs to be evaluated. Given the form of Eq. (4.11), this term is generally non-zero:

$$\left\langle \int_0^t u_\alpha(\tau) d\tau \int_0^t \zeta_\beta(\tau')\, d\tau' \right\rangle \delta_{\alpha\beta} = \int_0^t \int_0^t \langle u_\alpha(\tau) \zeta_\alpha(\tau') \rangle d\tau d\tau'.$$

This correlation $\langle u_\alpha(\tau)\zeta_\alpha(\tau')\rangle$ itself depends on the evolution of $\hat{u}$ and $\vec{r}_s$. For a general active particle in a spatially varying field, this term can be complex. However, if $\vec{\zeta}$ primarily originates from uncorrelated kicks independent of the swimmer's exact orientation and the direction at different times (except for the direct spatial dependency on $\hat{\mathbf{n}}$), and the director field $\hat{\mathbf{n}}$ evolves on timescales much slower than the noise correlation time (which is true for a static $\hat{\mathbf{n}}$), one might assume $\hat{u}$ and $\vec{\zeta}$ are uncorrelated for $t \neq t'$. More rigorously, this cross-correlation can be related to the fluctuation-dissipation theorem in active systems

or require specific assumptions about the stochastic process for $\hat{u}$. In many active particle models where translational noise $\vec{\zeta}$ is treated as purely external and $\hat{u}$ is determined by internal activity and rotational noise [21], this term is often neglected or assumes $\langle \hat{u}(t) \cdot \vec{\zeta}(t') \rangle = 0$. However, given the angular evolution Eq. (4.5) and given Eq. (4.11), it would contribute

$$2D_{Tn} \int_0^t \langle \hat{u}(\tau) \cdot \hat{n}(\vec{r}_s(\tau)) \rangle d\tau.$$

This would lead to another linear term in t if $\langle \hat{u} \cdot \hat{n} \rangle$ reaches a steady state average.

The form of $C_u(\vec{r}'_s - \vec{r}''_s, \tau)$ now depends on the interplay between the alignment dynamics in the FCD texture, driven by k, and the effect of the rotational noise D_R. If D_R is large, $C_u(\vec{r}'_s - \vec{r}''_s, \tau)$ will decay quickly (on the order of $1/D_R$), leading to a rapid crossover to diffusive behavior, as seen in the ABP model. If k is large compared to D_R, the swimmer will strongly align with the local director, and the decay of $C_u(\vec{r}'_s - \vec{r}''_s, \tau)$ will be largely determined by how quickly the director field $\hat{n}(\vec{r}_s(t))$ changes along the swimmer's path, and how well the swimmer maintains alignment despite rotational noise. Therefore, the MSD can exhibit rich crossover behavior between ballistic and diffusive regimes, influenced by v_s, D_T, D_A, D_R, k, and the geometric complexity of the FCDs. Numerical simulations are indispensable for exploring this complex interplay.

All this makes a full analytical solution for the MSD extremely challenging, if not impossible. The reasons are as follows:

1. Non-linear and coupled dynamics: The angular dynamics, Eq. (4.7), are inherently non-linear due to the $\sin(2\varphi)$ term. Furthermore, the angle $\varphi = \theta - \phi(\vec{r}_s(t))$ (see Figure 4.1) means that the orientation dynamics are coupled to the swimmer's position $\vec{r}_s(t)$ through the spatially dependent director angle $\phi(\vec{r}_s(t))$.

2. Spatially heterogeneous director field: The presence of FCDs means $\hat{\mathbf{n}}(\vec{r})$ is not uniform. The effective alignment experienced by the swimmer changes as it moves through the system. This breaks translational invariance, which is often a prerequisite for analytical tractability in active matter models [7, 29].

3. History dependence of orientation statistics: To calculate the orientation autocorrelation

$$C_u(\vec{r}'_s - \vec{r}''_s, \tau) = \langle \hat{u}(\vec{r}'_s, t) \cdot \hat{u}(\vec{r}''_s, t + \tau) \rangle,$$

we need to know the statistics of $\hat{u}(t)$, which itself depends on the history of $\vec{r}_s(t)$ through $\hat{n}(\vec{r}_s(t))$. This creates a feedback loop that is very hard to close analytically.

While a full analytical solution is out of reach, we can draw insights from simpler models.

If we set the alignment strength $k = 0$ (no interaction with the smectic) and only consider the active propulsion $v_s\hat{u}(t)$ and the noises ($\vec{\zeta}(t)$ and $\eta(t)$), the MSD for a 2D ABP is well-known, as showed in Chapter 2, section 2.2.2.

For uniform director field ($\hat{n}$ constant) and $k > 0$, the $\sin(2\varphi)$ term would act as a restoring torque, trying to align $\hat{u}$ with $\hat{n}$. This competition between alignment and rotational noise would lead to a modified effective D_R in the long-time limit, or potentially even more complex dynamics if the swimmer gets "trapped" in a specific orientation. However, a full analytical solution for this case still typically requires approximations.

Parallel and Perpendicular Components of the MSD

In a smectic system, particularly inside FCDs, the swimmer dynamics is highly anisotropic due to the underlying layered structure. We define the mean-square displacement components:

$$\langle \Delta r_{\parallel}^2(t) \rangle = \left\langle [\Delta \vec{r}_s(t) \cdot \hat{n}]^2 \right\rangle, \tag{4.23}$$

$$\langle \Delta r_{\perp}^2(t) \rangle = \left\langle |\Delta \vec{r}_s(t) - (\Delta \vec{r}_s(t) \cdot \hat{n})\, \hat{n}|^2 \right\rangle. \tag{4.24}$$

In the ideal smectic-A phase, $\hat{n} = \hat{z}$ and layers are flat, so the parallel direction corresponds to the normal to layers (inter-layer motion), and the perpendicular direction is in-plane (intra-layer motion). Due to high compressional rigidity (B), motion across layers is energetically unfavorable, leading to:

$$\langle \Delta r_{\parallel}^2(t) \rangle \ll \langle \Delta r_{\perp}^2(t) \rangle \tag{4.25}$$

this inequality arises from the intrinsic anisotropy of the smectic-A phase. In the ideal smectic-A configuration, the director field is uniform and points along the layer normal, $\hat{\mathbf{n}} = \hat{z}$. As a result, the parallel direction corresponds to motion across the smectic layers, while the perpendicular direction lies within the layers. Although the alignment energy, Eq. (4.6), favors the swimmer's orientation $\hat{u}(t)$ to align with $\hat{\mathbf{n}}$, actual translational motion across layers is energetically unfavorable

due to the high compressional modulus B. This suppresses inter-layer displacement regardless of the particle's instantaneous orientation. Consequently, while the particle may align along $\hat{z}$, it remains effectively confined within layers, where both active propulsion and translational diffusion are less hindered. This leads to highly anisotropic dynamics, with much faster transport in the plane of the layers than across them.

However, in focal conic domains, the local $\hat{n}(\vec{r})$ varies smoothly and nontrivially in space, curving and organizing layers into nested conic structures. This introduces complex guidance and trapping effects in swimmer trajectories. Analytically evaluating $\langle(\Delta\vec{r}_s \cdot \hat{n})^2\rangle$ or $\langle(\Delta\vec{r}_s \cdot \hat{n}_\perp)^2\rangle$ becomes infeasible as explained before for total MSD.

Implications for MSD in FCDs (2D)

When an active particle moves within a complex two-dimensional focal conic domain (FCD) texture, the MSD exhibits rich temporal behavior that reflects the interplay between activity, alignment, and the anisotropic geometry of the smectic structure. At short times, the swimmer typically exhibits ballistic motion, as it self-propels with speed v_s before experiencing significant reorientation or encountering substantial distortions in the director field. At intermediate times, the MSD behavior becomes highly nontrivial. Depending on the alignment strength k, rotational noise D_R, and the geometric configuration of the FCDs, the swimmer may follow director lines, become guided through curvature-enhanced pathways, or get transiently trapped in regions of high curvature or near defect cores. In such cases, the MSD may exhibit superdiffusive scaling if the texture promotes channel-like trajectories, or subdiffusive scaling if confinement dominates. At long times, especially under periodic boundary conditions or in large systems, the swimmer is expected to explore all orientations, leading to a crossover to normal diffusion. However, the effective diffusion coefficient will still carry the imprint of the underlying FCD structure and depends non-trivially on parameters such as v_s, D_T, D_A, D_R, k, and the spatial organization of the FCDs, including their density, defect type, and characteristic length scales.

Extension to 3D

Extending the model to three dimensions significantly increases both the complexity of the angular dynamics and the analysis of the resulting MSD. In three

dimensions, the orientation of the swimmer $\hat{u}(t)$ must be described by two angular variables (e.g., polar and azimuthal angles), and the stochastic torque $\boldsymbol{\eta}(t)$ becomes a three-component vector representing rotational noise. The evolution equation $\dot{\hat{u}} = k(\hat{u}\cdot\hat{\mathbf{n}})\,[\hat{\mathbf{n}} - (\hat{u}\cdot\hat{\mathbf{n}})\hat{u}] + \boldsymbol{\eta}(t)$ must be projected onto an orthonormal basis perpendicular to $\hat{u}$ to ensure the constraint $\hat{u}^2 = 1$ is preserved, making the dynamics inherently nonlinear. Furthermore, FCDs in 3D are geometrically more intricate than in 2D, comprising confocal ellipses and hyperbolas as focal lines, and resulting in a director field $\hat{\mathbf{n}}(\vec{r})$ that is fully three-dimensional and challenging to construct or visualize. Translational noise also becomes anisotropic in 3D and depends on the spatial orientation of $\hat{n}$, requiring a full tensorial treatment of the noise correlations. Finally, the correlation function for the rotational noise must be carefully defined to remain consistent with the projection constraint. Due to these complexities (nonlinear orientation dynamics, a spatially heterogeneous and anisotropic director field, and the geometry of 3D FCDs) analytical solutions become even more inaccessible than in 2D. As such, numerical simulations are not only useful but essential to fully characterize the transport and MSD behavior of active particles in 3D smectic environments. However, in this work we will focus in 2D systems.

4.2 ABP Simulation in Smectic Liquid Crystals

This section details the numerical simulation approach used to investigate the dynamic behavior of ABP within a smectic-A (SmA) liquid crystal environment, specifically in the presence of FCDs.

In this work, we focus on the two-dimensional (2D) behavior of active particles. The continuous stochastic differential equations, Eq. (4.1), governing the dynamics of an ABP in a general potential and anisotropic medium are discretized using a numerical integration scheme. Assuming the overdamped limit, where inertial effects are negligible (as justified by the small mass and high viscosity at the microscale), the continuous Langevin equations for the particle's position $\vec{r}_s(t)$ and orientation $\theta(t)$ (implicitly accounting for the active force and the alignment with the local smectic director) can be numerically integrated using a simple Euler-Maruyama scheme.

The discretized equations for the particle's position $\vec{r}(t) = (x(t), y(t))$ and its

orientation $\theta(t)$ are:

$$\vec{r}_s(t+\Delta t) = \vec{r}_s(t) + v_s\hat{u}(t)\Delta t + \vec{\xi}(t), \tag{4.26}$$

$$\theta(t+\Delta t) = \theta(t) - \frac{1}{2}k\sin(2\varphi(t))\Delta t + \sqrt{2D_R\Delta t}\eta(t). \tag{4.27}$$

Here, Δt is the discrete time step, and the terms are interpreted as follows:

- $\vec{r}(t)$ and $\theta(t)$: The particle's position and orientation angle at time t.
- $v_s\hat{u}(t)\Delta t$: This is the deterministic self-propulsion displacement. v_s is the constant self-propulsion speed of the active particle, and $\hat{u}(t) = (\cos\theta(t), \sin\theta(t))$ is the unit vector representing the particle's instantaneous internal propulsion direction. This term accounts for the ballistic component of the active motion.
- $\vec{\xi}(t)$: This represents the anisotropic translational noise. In a homogeneous isotropic fluid, this would be a simple thermal noise term. However, in our smectic liquid crystal environment, the translational diffusion of the particle is anisotropic, meaning it diffuses differently parallel versus perpendicular to the local smectic director. This term effectively incorporates both isotropic thermal diffusion (D_T) and an additional active-like anisotropic diffusion (D_A) perpendicular to the local director. It is generated from independent Gaussian random numbers and scaled appropriately by the square root of the diffusion coefficients and time step,

$$\vec{\xi}(t) = (\sqrt{2(D_T + D_A)\Delta t}\xi_{\parallel}, \sqrt{2D_T\Delta t}\xi_{\perp}).$$

- $-\frac{1}{2}k\sin(2\varphi(t))\Delta t$: This is the deterministic torque due to alignment with the local smectic director. The coupling constant k determines the strength of this aligning torque. $\varphi(t) = \theta(t) - \phi(\vec{r}(t))$ is the instantaneous relative angle between the particle's orientation $\theta(t)$ and the local orientation of the smectic director $\phi(\vec{r}(t))$ at the particle's position, see Figure 4.1. The $\sin(2\varphi)$ form arises from the quadrupolar nature of typical nematic/smectic alignment, favoring alignment of the particle's long axis (or propulsion axis) either parallel ($\varphi = 0$) or perpendicular ($\varphi = \pi/2$) to the director. Here, we assume parallel alignment with the director $k > 0$. This term ensures the active particle tends to align with the local orientation of the smectic layers or director field.

- $\eta(t)$: This represents the rotational noise term, accounting for thermal fluctuations that cause the particle's orientation to randomly change. It is drawn from a Gaussian distribution and scaled by the rotational diffusion coefficient D_R and time step, $\sqrt{2D_R\Delta t}$.

4.2.1 Implementation of the Simulation Algorithm

Our simulation is implemented using Python, leveraging the NumPy library for efficient numerical operations on arrays. The core of the simulation is encapsulated within the `ABP_SmA_2D` function, which performs the time-stepping integration of the discretized Langevin equations.

The `ABP_SmA_2D` function takes several input parameters to define the simulation environment and particle properties, as show in Figure 4.2.

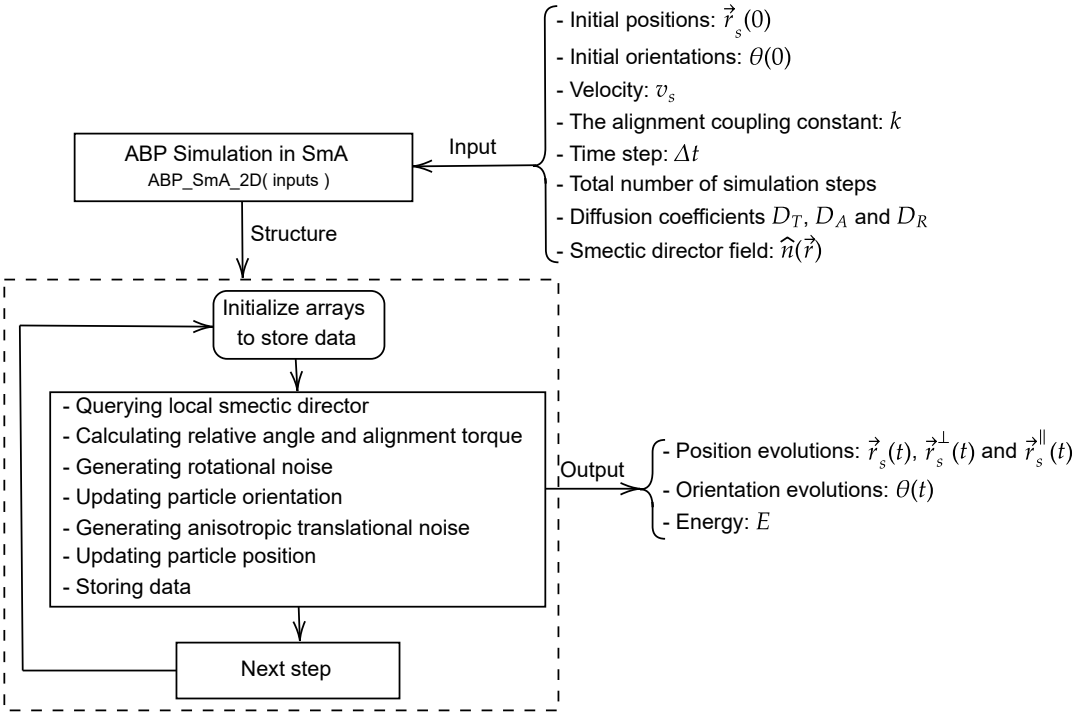

Figure 4.2: Diagram of the ABP_SmA_2D function for the ABP simulation.

The simulation then proceeds in a loop over discrete time steps. Within each step, the following operations are performed for all particles simultaneously (vectorized using NumPy):

1. **Querying local smectic director:** At each time step, the local orientation of the smectic director $\hat{\mathbf{n}}(\vec{r}_s(t))$ is evaluated at the particle's current position

$\vec{r}_s(t)$. To implement periodic boundary conditions, the position is mapped onto the finite simulation grid using the modulo operator (`%N`), ensuring that the particle interacts consistently with the periodically extended director field. The x and y components of the director at the corresponding grid cell are extracted and normalized to maintain unit magnitude, $\|\hat{\mathbf{n}}\| = 1$. Although the director field is discretized on a finite grid, this approximation is well-justified in the thermodynamic limit: as the system size increases and the grid resolution becomes finer, the particle's position becomes indistinguishable from the nearest grid point. Thus, the value of the director field sampled at the nearest grid cell becomes an accurate representation of the continuous field at the particle's actual position. This ensures that the dynamics remain faithful to the intended continuum model, even with discrete numerical implementation.

2. **Calculating relative angle and alignment torque:** The relative angle $\varphi(t) = \theta(t) - \phi(\vec{r}_s(t))$ between the particle's orientation and the local smectic director is calculated and normalized to be within $[-\pi, \pi]$. This ensures consistent behavior of the sinusoidal alignment torque. The deterministic alignment torque, $-\frac{1}{2}k\sin(2\varphi(t))$, is then calculated. This torque acts to minimize the alignment energy, favoring configurations where $\varphi = 0$ or $\varphi = \pi$ (particle aligned parallel to director) or $\varphi = \pi/2$ (particle aligned perpendicular to director), depending on the sign of k. For $k > 0$, parallel alignment is favored.

3. **Updating particle orientation:** The particle's orientation $\theta(t)$ is updated using the Euler-Maruyama scheme:

$$\theta(t + \Delta t) = \theta(t) - \frac{1}{2}k\sin(2\varphi(t))\Delta t + \sqrt{2D_R\Delta t}\eta(t).$$

   This step incorporates both the deterministic alignment torque and random thermal reorientations.

4. **Generating anisotropic translational noise:** Translational noise for each particle is generated in two components: one parallel to the local smectic director and one perpendicular to it. This is crucial for capturing the anisotropic diffusion in smectic environments.

   - Two independent standard normal random numbers are generated for

each particle.

- These are scaled by $\sqrt{2(D_T + D_A)\Delta t}$ for parallel and $\sqrt{2D_T\Delta t}$ for perpendicular components.

5. **Updating particle position:** The particle's position $\vec{r}_s(t)$ is updated using the Euler-Maruyama scheme, incorporating the self-propulsion and the generated anisotropic noise:

$$\vec{r}_s(t + \Delta t) = \vec{r}_s(t) + v_s\hat{u}(t)\Delta t + \vec{\xi}(t).$$

6. **Storing data:** At the end of each step, the updated positions, orientations, alignment energies, and the local smectic director components are stored for subsequent analysis.

This iterative process allows us to trace the trajectories of a large ensemble of active particles as they move through the pre-defined, FCD patterns.

4.2.2 Analysis of Particle Dynamics: Mean Squared Displacement

To quantitatively characterize the transport properties of the active particles in the smectic environment, we compute various forms of the MSD. The MSD provides insight into how a particle's position or orientation spreads over time and is a key metric for distinguishing different diffusion regimes (e.g., ballistic, diffusive, anomalous).

Total MSD

The total MSD, $\langle \Delta r^2(t) \rangle$, measures the average squared displacement of particles from their initial positions over time. It is calculated following Eq. (4.14). The ensemble average $\langle \dots \rangle$ is computed over all simulated particles. This provides a general overview of particle spreading.

Parallel and Perpendicular MSD ($\langle \Delta r_{\parallel}^2 \rangle$ and $\langle \Delta r_{\perp}^2 \rangle$)

In an anisotropic medium like a smectic liquid crystal, the overall MSD can obscure crucial details about how particles move along different directions relative to the local order. Therefore, we calculate the MSD components parallel ($\langle \Delta r_{\parallel}^2(t) \rangle$)

and perpendicular ($\langle \Delta r_{\perp}^2(t) \rangle$) to the local smectic director field. This approach leverages the stored local director information for each particle at every time step.

For each particle's displacement vector $\Delta \vec{r}_s(t) = \vec{r}_s(t) - \vec{r}_s(0)$, we project it onto the local smectic director $\hat{\mathbf{n}}(\vec{r}(t))$ and the direction perpendicular to it, $\hat{\mathbf{n}}_{\perp}(\vec{r}(t))$. The parallel and perpendicular MSD component is computed following the Eqs. (4.23) and (4.24), respectively. This measures the average squared displacement parallel and transverse to the local orientation of the smectic layers/director. Here, $\hat{\mathbf{n}}_{\perp}(\vec{r}_(t))$ is a unit vector orthogonal to $\hat{\mathbf{n}}(\vec{r}(t))$ in the 2D plane (e.g., if $\hat{\mathbf{n}} = (n_x, n_y)$, then $\hat{\mathbf{n}}_{\perp} = (-n_y, n_x)$).

This separation is critically important for our thesis because:

- It directly quantifies the anisotropic transport induced by the smectic environment and the FCDs. We can observe if particles diffuse faster or slower along specific directions.
- It allows for the detection of anomalous diffusion, such as the logarithmic growth in transverse MSD predicted for active swimmers in smectics. The $\langle \Delta r_{\perp}^2(t) \rangle$ component is precisely where such effects would manifest, indicating movement that is highly constrained across the layers.
- It provides insights into how the specific geometry of FCDs, with their varying layer curvature and director orientation, modulates particle movement by preferentially guiding or hindering motion along or across the local director field.

Rotational Mean Squared Displacement (RMSD)

The RMSD ($\langle \Delta\theta^2(t) \rangle$) is another valuable metric for characterizing the rotational dynamics of the active particles. It measures the average squared change in the particle's orientation relative to its initial orientation:

$$\langle \Delta\theta^2(t) \rangle = \left\langle (\theta(t) - \theta(0))^2 \right\rangle . \tag{4.28}$$

This quantifies how quickly the particle's orientation randomizes over time due to both rotational diffusion and the aligning torque from the smectic director.

4.2.3 Computational Details

The simulation is performed for an ensemble of active particles to ensure robust statistical averages. The orientation of each particle evolves according to stochastic dynamics coupled to the background smectic director field $\hat{\mathbf{n}}(\vec{r})$, which remains fixed throughout the simulation. We considered two types of SmA environments: one with a nearly "flat" configuration (uniform $\hat{\mathbf{n}}$), were obtained from the data in Liarte's work [17], and another with mimetic FCDs (see Appendix A), texture. The latter includes concentric circular domains in 2D (labeled 1 through 4). By fixing the smectic field, our simulations isolate the influence of geometric anisotropy and director curvature on the dynamics of the active particles, avoiding feedback from particle-induced distortions and allowing for a clear exploration of passive–active coupling effects.

To simulate the dynamics, we initialized an ensemble of $N = 500$ particles, which is sufficient to obtain statistically convergent results for key observables such as the MSD. The numerical time step was set to $\Delta t = 0.01$, small enough to resolve the fastest dynamical timescales in the system, including the rotational diffusion time $1/D_R$, the alignment relaxation time $1/k$, and the persistence time L_p/v_s, where L_p is the persistence length of the trajectory. The total simulation time was either $T = 2000$ or $T = 4000$, depending on the observed MSD behavior: longer durations were used when the system exhibited slow relaxation, subdiffusion, or transient trapping.

Importantly, we systematically varied the propulsion speed and the coupling strength to the smectic texture. In particular, we explored $v_s = 1, 3, 6$ and $k = 1, 3, 6$, for both flat and FCD configurations. These variations allow us to probe the full range of dynamical regimes, from weak to strong alignment, and from slow to fast swimmers, and to investigate how these parameters modulate transport in anisotropic and heterogeneous environments. This computational framework offers a controlled setting to study the emergence of anisotropic diffusion, alignment-induced trapping, and possible guidance effects in active systems embedded in structured liquid-crystalline media.

4.3 Analysis of ABP Dynamics in Smectic-A Environments

This section presents and discusses the results obtained from our numerical simulations of ABPs navigating within a static smectic-A (SmA) liquid crystal environment. We investigate two primary configurations of the SmA phase: a simple "flat" (uniform) director field and a complex field structured by mimetic FCDs. Our analysis focuses on the MSD, distinguishing between its total, parallel, and perpendicular components, as well as the RMSD, to comprehensively characterize the anisotropic transport properties of the ABPs.

4.3.1 SmA with "Flat" Configuration

In a flat SmA configuration, our smectic director field $\hat{\mathbf{n}}$ is approximately uniform across the entire simulation domain. This serves as a fundamental benchmark, allowing us to understand the behavior of ABPs under anisotropic translational noise and a constant alignment torque, before introducing the complexities of a spatially varying director field.

Figure 4.3 illustrates a typical trajectory of an ABP in a flat SmA configuration. The green dot marks the particle's initial position (randomly defined), and the red line depicts its trajectory. As expected from the alignment coupling constant k in our model, the particle exhibits a strong preference to align and move along the direction of the smectic director field $\hat{\mathbf{n}}$. This alignment occurs because the quadratic coupling term in the alignment energy, proportional to $-k(\hat{\mathbf{u}} \cdot \hat{\mathbf{n}})^2$, drives the particle's orientation $\hat{\mathbf{u}}$ towards the local director $\hat{\mathbf{n}}$, thereby minimizing the system's energy. However, the presence of rotational noise $\eta(t)$ (with strength determined by D_R) continuously perturbs the particle's orientation. This competition leads to characteristic persistent motion at short times, followed by diffusive-like behavior at longer times, indicating a loss of memory of the initial propulsion direction.

The total MSD for different coupling strengths k and self-propulsion velocities v_s is presented in Figure 4.4.

- **Effect of alignment coupling (k):** As observed in the left panel of Figure 4.4, for smaller values of the alignment coupling constant k, the total MSD exhibits a shorter crossover time (τ_{cross}) from ballistic ($\propto t^2$) to diffusive ($\propto t$) behavior. The crossover time for an ABP marks the transition from directed,

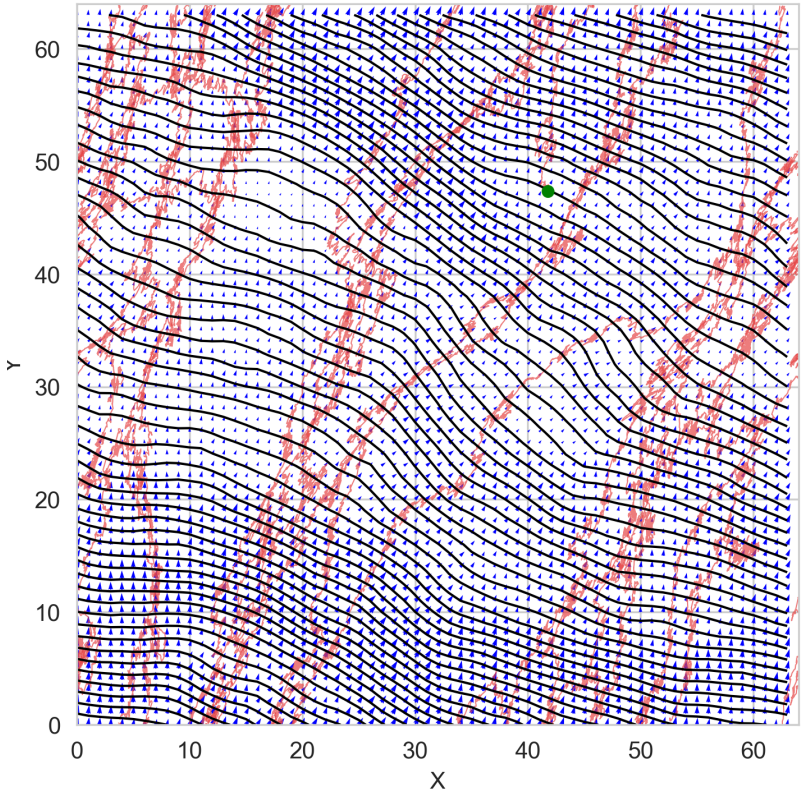

Figure 4.3: Behavior of an ABP in a flat configuration of SmA. The green dot indicates the initial position, and the red line represents the particle's trajectory.

persistent motion to a random walk dominated by rotational diffusion. A weaker coupling k implies that the alignment torque is less effective in maintaining the particle's orientation, allowing rotational noise to more rapidly randomize the particle's propulsion direction. This reduction in persistence leads to an accelerated transition to a standard diffusive regime at longer times, where $\langle \Delta r^2(t) \rangle \propto t$. This finding is consistent with general principles of active matter, where strong alignment enhances particle persistence and, consequently, its effective diffusion coefficient [21].

- **Effect of self-propulsion velocity (v_s):** The right panel of Figure 4.4 shows the total MSD for varying v_s (with fixed $k = 3$). At short times, the MSD clearly displays a quadratic dependence on time ($\propto t^2$), characteristic of ballistic motion, reflecting the directed self-propulsion of the active particle. At longer times, the MSD transitions to a linear regime, indicative of diffusive behavior. Crucially, increasing v_s leads to a significantly higher effective diffusion coefficient in this long-time limit. This enhanced long-time diffusion, where D_{eff} scales with v_s^2, is a well-known hallmark of active particles in

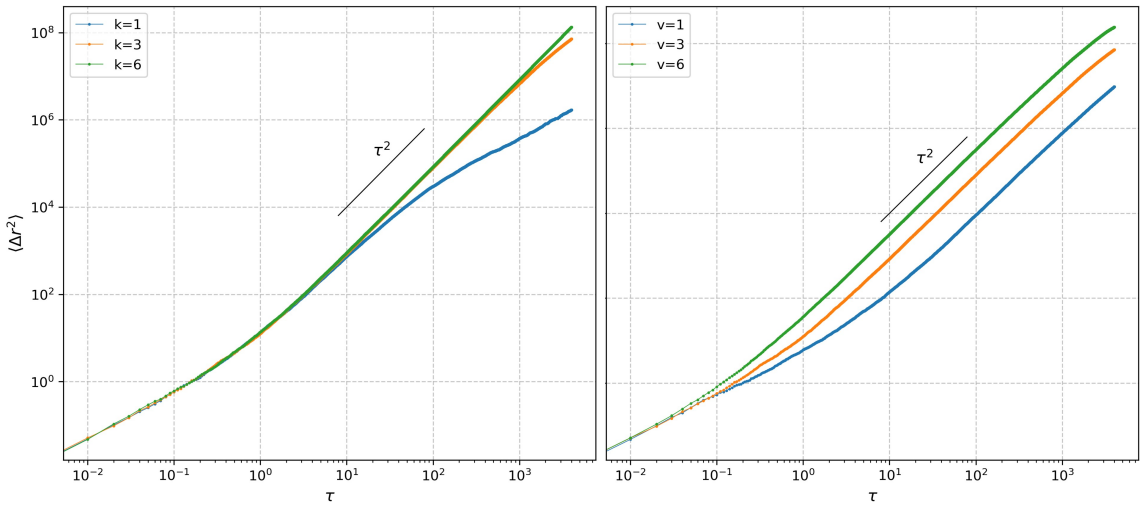

Figure 4.4: Total MSD for varying coupling strengths k and self-propulsion velocities v_s. The left panel shows results with fixed $v_s = 3$ and varying k, while the right panel shows fixed $k = 3$ with varying v_s.

isotropic media [3]. Our results in the flat smectic background, therefore, confirm this fundamental aspect of ABP dynamics, demonstrating that even in an anisotropic medium, the basic enhanced diffusion mechanism persists.

Figure 4.5 displays the RMSD, $\langle \Delta\theta^2(t) \rangle$, for different values of the coupling constant k. For all values of k, the RMSD initially exhibits a superdiffusive scaling, approximately $\tau^{1.35}$. This transient superdiffusive behavior at short times can be attributed to the rapid relaxation of the randomly chosen initial particle orientations towards alignment with the fixed smectic director. The strong deterministic alignment torque quickly reduces the initial large angular deviations. For larger values of k, a plateau-like region appears, where $\langle \Delta\theta^2(t) \rangle$ remains relatively constant for an extended period. This plateau signifies that the particle's orientation is strongly "locked" to the director, with its relative angle φ fluctuating minimally around zero. Any changes in the particle's absolute orientation θ are primarily a result of the director's own orientation (which is fixed in this flat configuration) and small angular excursions due to rotational noise that do not lead to significant deviations from the initial alignment. Finally, at long times, the RMSD transitions to a linear regime ($\propto t$), which is solely governed by the rotational diffusion coefficient D_R. In this phase, rotational noise eventually randomizes the particle's absolute orientation, even when strongly aligned. The stronger the coupling k, the longer it takes for this linear, diffusive regime to fully manifest, as the deterministic alignment torque more effectively resists the influence of rotational noise.

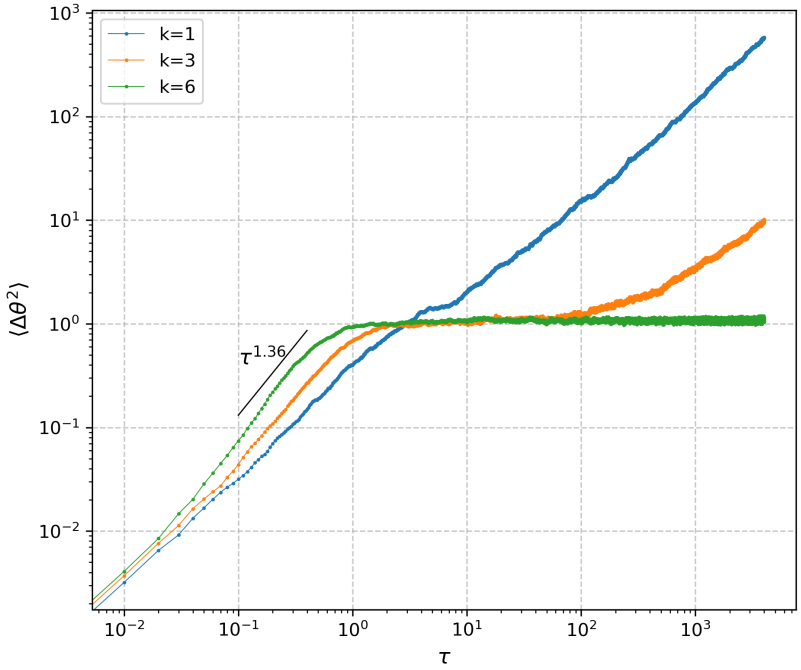

Figure 4.5: RMSD for different values of coupling k in a flat SmA configuration.

Figure 4.6 illustrates the parallel ($\langle \Delta r_{\parallel}^2 \rangle$) and perpendicular ($\langle \Delta r_{\perp}^2 \rangle$) components of the MSD in the flat SmA configuration.

- **Perpendicular MSD ($\langle \Delta r_{\perp}^2 \rangle$):** The perpendicular MSD consistently exhibits a linear scaling with time ($\propto t$) across all tested parameters. This behavior is primarily driven by the isotropic translational noise (D_T) in the perpendicular direction. In a fixed, flat, and homogeneous SmA director field, there is no active propulsion component perpendicular to the director. Therefore, the transverse spreading is dominated by standard thermal diffusion. This finding contrasts with some studies on active matter in smectic-like environments [25, 12] that report subdiffusive (e.g., logarithmic) behavior in the transverse direction. Such subdiffusivity typically arises from either strong active layer deformations induced by the swimmer or specific noise models that restrict transverse motion across deformable layers. Our model, featuring a static and rigid flat SmA director field, does not exhibit these collective layer fluctuations or active deformations, thus allowing for straightforward diffusive spreading perpendicular to the director.

- **Parallel MSD ($\langle \Delta r_{\parallel}^2 \rangle$):** The parallel MSD shows behavior strikingly similar to the total MSD. This is physically expected: in a flat SmA configuration, the particle's self-propulsion $v_s \hat{\mathbf{u}}(t)$ is preferentially aligned with the global

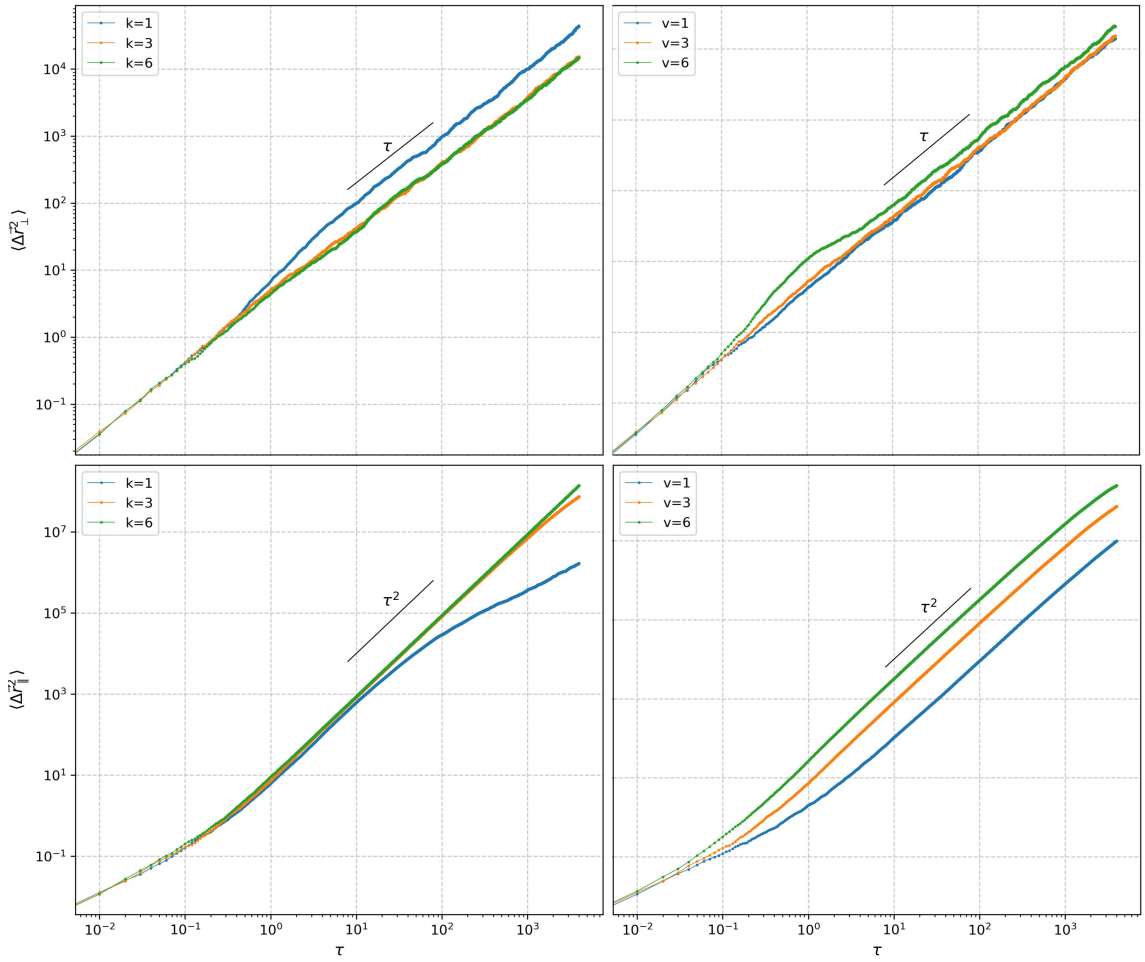

Figure 4.6: Perpendicular and parallel MSD for different values of coupling k and velocities v_s in a flat SmA configuration. The left panel shows results with fixed $v_s = 3$ and varying k, while the right panel shows fixed $k = 3$ with varying v_s.

director $\hat{\mathbf{n}}$ due to the strong coupling k. Consequently, the dominant contribution to the particle's long-time displacement and enhanced diffusion comes from its persistent motion along this single, preferred direction. The total MSD is the sum of the squared displacements along orthogonal components ($\langle \Delta r^2(t) \rangle = \langle \Delta r^2_{\parallel}(t) \rangle + \langle \Delta r^2_{\perp}(t) \rangle$). Since the active, directed motion in the parallel direction leads to significantly larger displacements than the purely diffusive motion in the perpendicular direction, $\langle \Delta r^2_{\parallel} \rangle$ will dominate the total MSD, hence their close resemblance. This observation confirms that the active transport is primarily channeled along the director field in a uniform smectic environment.

4.3.2 SmA with mimetic FCDs

Next, we investigate the more complex scenario where ABPs interact with a SmA director field structured by mimetic FCDs. As discussed in Chapter 3, FCDs are characterized by smectic layers forming singularities, with the director field $\hat{\mathbf{n}}$ pointing radially outward or inward from these singularities. These domains introduce significant spatial heterogeneity and curvature into the director field, fundamentally altering the environment for active swimmers.

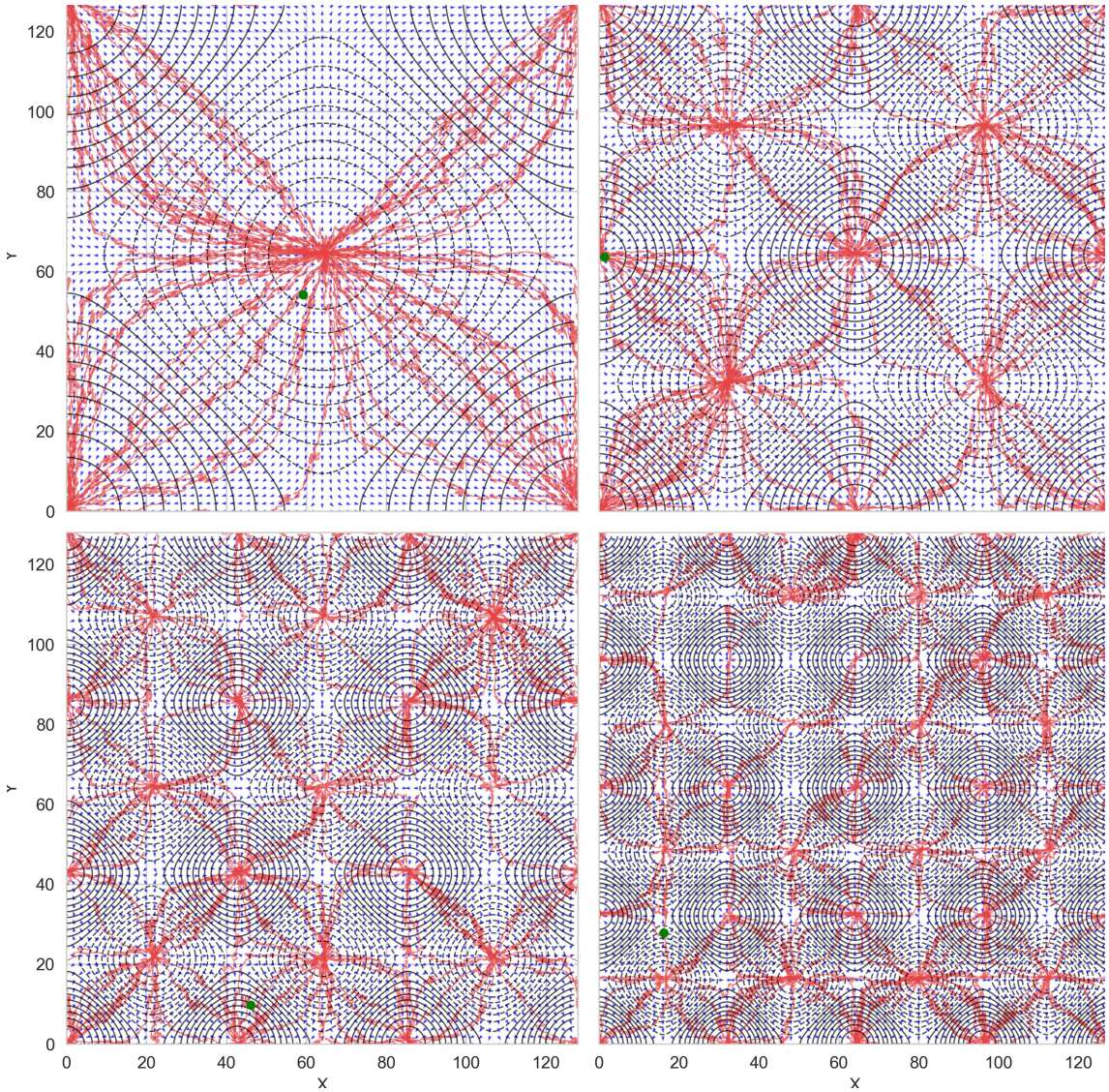

Figure 4.7: Behavior of an ABP in SmA with 1, 2, 3, and 4 mimetic FCDs. Green dots indicate initial positions, and red lines show particle trajectories.

The total MSD at short times exhibits a ballistic behavior ($\propto \tau^2$) and a linear behavior at long times, as shown in Figure 4.8. This general trend is expected

for active Brownian particles. However, the total MSD inherently convolves information from both parallel and perpendicular components of motion. For a deeper understanding of the anisotropic transport within the highly structured FCD environment, it is therefore crucial to analyze the MSD components parallel and perpendicular to the local director, as they provide distinct insights into how the active particle interacts with and navigates the smectic layers and defect structures.

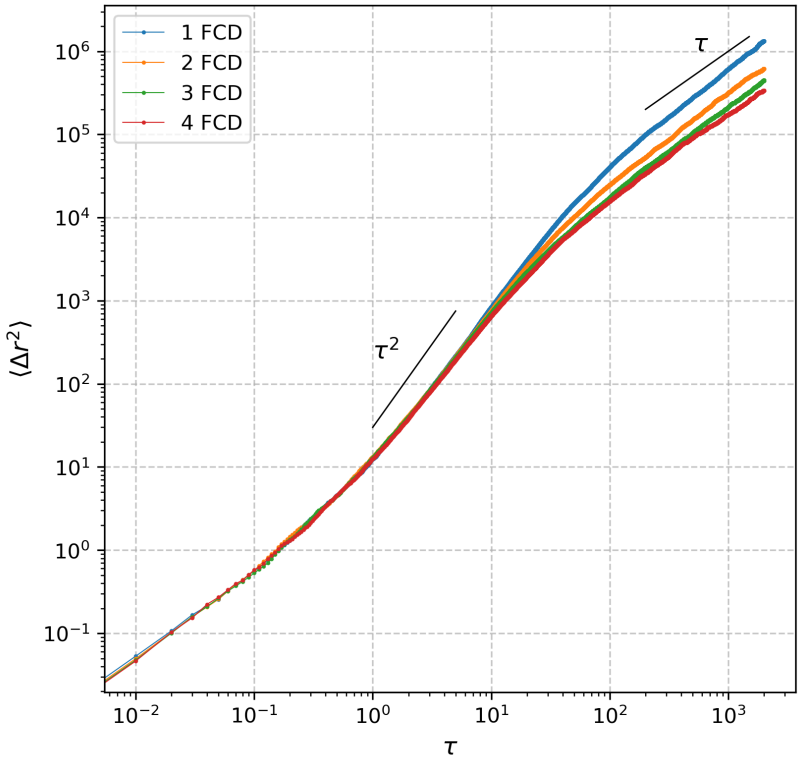

Figure 4.8: Total MSD for different configurations of SmA with 1, 2, 3, and 4 mimetic FCDs ($v_s = 3$ and $k = 3$).

Figure 4.7 illustrates sample trajectories of ABPs within SmA configurations featuring 1, 2, 3, and 4 FCDs, with fixed parameters $k = 3$ and $v_s = 3$. The green dot denotes the initial particle position, and red lines show the trajectories.

We observe that the particles strongly align with the local director $\hat{\mathbf{n}}$ of the SmA due to the coupling term k, which dictates a preferred direction of motion. This causes them to momentarily move towards the singularity (center) of the FCDs. However, upon reaching or closely approaching the singularity, the particle's orientation becomes effectively random. This reorientation at the singularity is a complex interplay of several factors: the director field becomes ill-defined or rapidly changing near the singular point, leading to strong and potentially chaotic

alignment torques; the quadratic nature of the alignment energy $(\hat{\mathbf{u}} \cdot \hat{\mathbf{n}})^2$ implies that the particle equally prefers aligning parallel or anti-parallel to $\hat{\mathbf{n}}$, and rotational noise can easily induce a flip between these states, especially in regions of low director coherence; and the high curvature of layers near the singularity effectively "scatters" the particle's orientation, disrupting its persistent motion. These FCD singularities thus act as reorientation centers, introducing an additional, spatially localized mechanism that randomizes the particle's direction of motion. Globally, this leads to more circuitous and less persistently directed trajectories compared to the flat configuration.

Figure 4.9 displays the perpendicular MSD, $\langle \Delta r_\perp^2 \rangle$, for various numbers of FCDs. At short times, $\langle \Delta r_\perp^2 \rangle$ exhibits a superdiffusive scaling, approximately

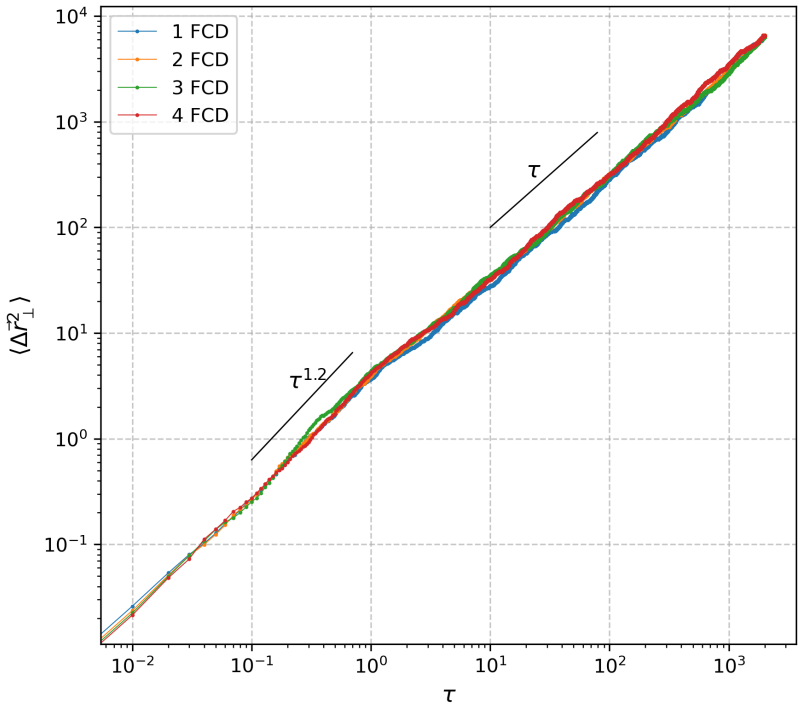

Figure 4.9: Perpendicular MSD for different configurations of SmA with 1, 2, 3, and 4 mimetic FCDs ($v_s = 3$ and $k = 3$).

$\tau^{1.2}$. This initial superdiffusive behavior in the perpendicular component, even with a linear diffusion coefficient D_T for thermal noise, is a direct consequence of the particle's persistent (ballistic) motion combined with the spatial curvature of the FCD director field. As the particle propagates, its velocity vector $\hat{\mathbf{u}}(t)$ aligns with the local director $\hat{\mathbf{n}}(\vec{r}(t))$. However, as $\hat{\mathbf{n}}(\vec{r}(t))$ continuously changes direction due to the curvature within the FCD, the component of the particle's overall persistent displacement projected onto the local perpendicular direction

at each moment can accumulate faster than pure diffusion. This anomalous short-time behavior in the transverse component is a signature of active particles navigating highly structured and curved environments. At longer times, the $\langle \Delta r_{\perp}^2 \rangle$ consistently transitions to a linear scaling with time. This indicates that, over extended periods, the perpendicular movement is dominated by diffusion, primarily due to the constant translational noise D_T and the accumulated effects of random reorientations (both rotational noise and scattering by FCD singularities).

The most interesting behavior is observed in the parallel MSD, $\langle \Delta r_{\parallel}^2 \rangle$, as shown in Figure 4.10. At short times, $\langle \Delta r_{\parallel}^2 \rangle$ clearly shows ballistic behavior ($\propto \tau^2$),

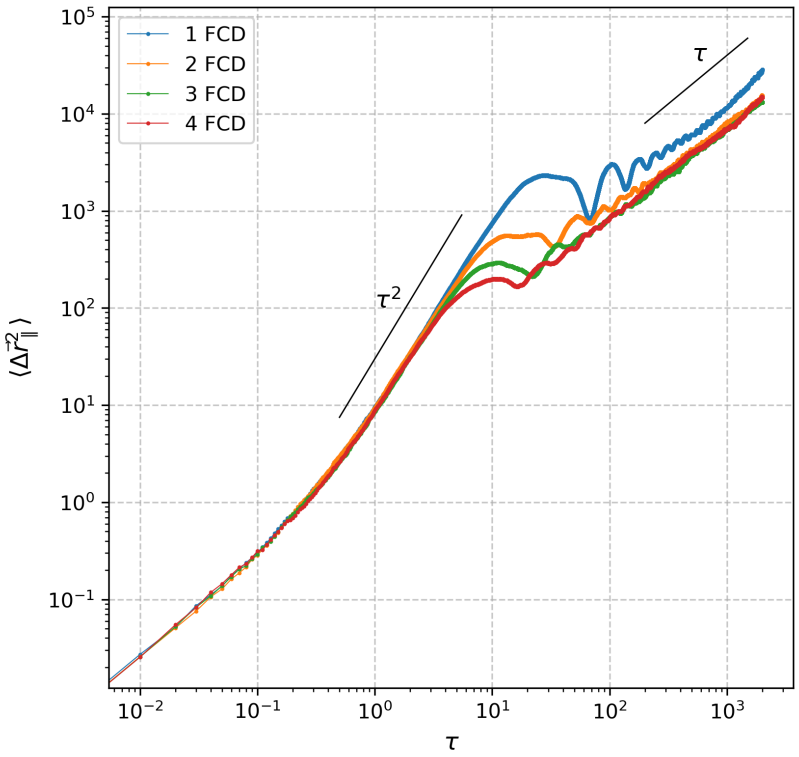

Figure 4.10: Parallel MSD for different configurations of SmA with 1, 2, 3, and 4 mimetic FCDs ($v_s = 3$ and $k = 3$).

characteristic of the self-propulsion of the active particle. Following this initial ballistic regime, the MSD exhibits a remarkable oscillatory pattern. The extent and damping of these oscillations depend on the number of FCDs present in the system. For a single FCD (blue line in Figure 4.10), the oscillation persists for a longer duration before $\langle \Delta r_{\parallel}^2 \rangle$ finally transitions to a linear, diffusive behavior at very long times. It is possible that these oscillations are an artifact of limited statistics for our simulations. We are currently checking this point, or whether there is a plausible interpretation for them.

Figure 4.11 presents the RMSD, $\langle \Delta\theta^2(t) \rangle$, for different numbers of FCDs. The

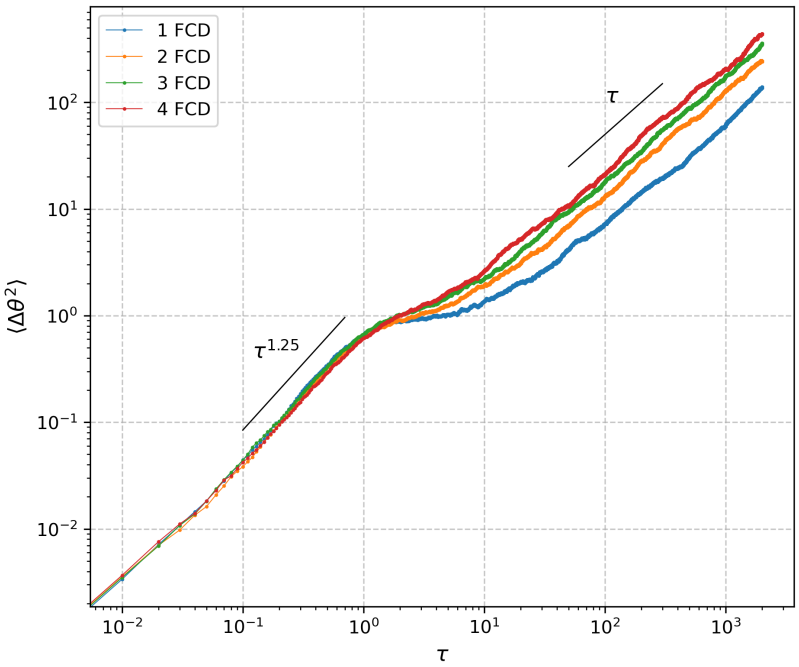

Figure 4.11: RMSD for different configurations of SmA with 1, 2, 3, and 4 mimetic FCDs ($v_s = 3$ and $k = 3$).

RMSD in FCD environments exhibits a qualitatively similar behavior to that observed in the flat configuration. There is an initial superdiffusive regime, followed by a plateau (or region of slower growth for larger k) due to strong alignment, and finally a linear scaling at long times. The fundamental rotational dynamics, governed by D_R and the alignment torque strength k, remain dominant. While the spatially varying director field in FCDs introduces more complex local reorientation dynamics, the ensemble-averaged RMSD still reflects the overall random particle orientation due to noise and alignment relaxation. The presence of FCD singularities, acting as additional local reorientation centers, contributes to the stochastic process, potentially influencing the crossover times or the precise magnitude of the long-time rotational diffusion compared to the flat case, but the general shape of the RMSD curve is preserved.

Chapter 5

Conclusions and Outlook

5.1 Conclusions

In this thesis, we have performed comprehensive numerical simulations to investigate the dynamic behavior of active Brownian particles (ABPs) within smectic-A (SmA) liquid-crystal environments, focusing on both nearly flat (uniform) configurations and those structured by mimetic Focal Conic Domains (FCDs). Our analysis, primarily through the Mean Squared Displacement (MSD) and Rotational Mean Squared Displacement (RMSD), has revealed distinct transport features influenced by the interplay between active propulsion, alignment coupling with the director field, and the spatial anisotropy of the smectic medium.

For ABPs in a nearly flat SmA configuration, our simulations confirm fundamental aspects of active matter physics:

- We observed the characteristic transition from ballistic motion at short times to diffusive behavior at long times in the total MSD, consistent with predictions for ABPs in isotropic media [21, 3].
- The self-propulsion velocity (v_s) directly enhances the long-time effective diffusion coefficient, demonstrating the active nature of the particles.
- The alignment coupling constant (k) plays a crucial role in determining the persistence time; stronger coupling leads to longer ballistic regimes and enhanced effective diffusion by maintaining the particle's orientation along the fixed director.
- The perpendicular MSD ($\langle \Delta r_\perp^2 \rangle$) exhibits purely linear, diffusive scaling. This is a significant finding that differentiates our model from those where active particles induce layer deformations or are strongly confined by fluctuating layers, which can lead to subdiffusive or logarithmic behavior [25, 12]. In our model, with a equilibrium director field and the presence of rotational noise, the motion perpendicular to the director is dominated by thermal diffusion.

- The parallel MSD ($\langle \Delta r_{\parallel}^2 \rangle$) closely mirrors the total MSD, indicating that the active transport is predominantly channeled along the uniform director field.
- The RMSD transitions from an initial superdiffusive regime to a long-time linear diffusive regime, with a transient plateau for stronger alignment, demonstrating the competition between deterministic alignment and random rotational noise.

The introduction of mimetic FCDs significantly alters the ABP dynamics, revealing more intricate transport phenomena:

- We have established that FCD singularities act as effective reorientation centers for active particles. Upon approaching these singularities, the particle's orientation is reset due to the rapidly changing or ill-defined local director field and the quadratic nature of the alignment interaction. This scattering mechanism provides a spatially localized "noise" that disrupts the persistent motion.
- The perpendicular MSD ($\langle \Delta r_{\perp}^2 \rangle$) exhibits an initial superdiffusive regime (approximately $\tau^{1.2}$) before transitioning to linear diffusion. This anomalous short-time behavior arises from the particle's persistent motion being projected onto a continuously reorienting local perpendicular direction within the curved FCD environment.
- Most notably, the parallel MSD ($\langle \Delta r_{\parallel}^2 \rangle$) displays a remarkable oscillatory behavior at intermediate to long times, following an initial ballistic phase. If genuine (this behavior may be an artifact of limited statistics), these oscillations highlight a complex interplay between ballistic persistence and stochastic reorientation induced by the structured environment.
- The RMSD in FCDs qualitatively resembles that in the flat case, demonstrating that the fundamental rotational dynamics are still governed by intrinsic noise and alignment, but the FCD singularities contribute to the overall randomization process, potentially influencing crossover times.

In summary, this dissertation shows that the complex microstructure of smectic liquid crystals gives rise to intriguing and unexpected transport properties of active Brownian particles. The spatially varying director field and the presence of singularities introduce novel reorientation mechanisms that go beyond simple rotational diffusion, leading to rich, non-trivial MSD behaviors, especially the

oscillatory pattern in the parallel component. These findings highlight the importance of considering the detailed structure of anisotropic active environments for predicting and controlling active matter transport.

5.2 Outlook and Future Work

The results presented in this dissertation pave the way for several exciting developments for future research:

- **Exploring diverse FCD geometries:** Our study focused on mimetic FCDs. Future work could investigate ABPs in other types of FCDs, such as cylindrical (Type III) or classical (Type II, based on the elliptic-hyperbolic pair), or even more complex textures arising from various boundary conditions. Each FCD type possesses unique curvature and defect structures that would likely lead to distinct ABP dynamics.

- **Systematic parameter space exploration in FCDs:** A more exhaustive study of the influence of varying ABP parameters (v_s, D_T, D_A, D_R, k) in different FCD configurations would be valuable. Understanding how these intrinsic particle properties interact with the extrinsic environmental complexity is crucial.

- **Quantitative analysis of oscillations:** Delving deeper into the nature of the MSD oscillations in FCDs, including their amplitude, period, and damping rate as a function of FCD density, size, and ABP parameters, could provide more quantitative insights into the "scattering" mechanism by singularities. This could involve developing analytical approximations for effective reorientation rates within a textured field.

- **Three-dimensional (3D) simulations:** Extending the simulations to 3D would allow for a more realistic representation of smectic environments and FCDs, which are inherently 3D structures. This would introduce additional complexities in director field definition and particle dynamics.

- **Coupling to smectic dynamics:** A natural next step is to relax the assumption of a smectic director field and allow for particle-induced deformations and flows. This would involve coupling the ABP dynamics to the continuum equations of smectic hydrodynamics (e.g., Ericksen-Leslie-Parodi theory),

creating a truly active liquid crystal system where particles and the medium mutually influence each other. This is particularly relevant for understanding phenomena like active turbulence in liquid crystals or self-organization of active particles by collective interactions with the fluid.

- **Collective behavior of multiple ABPs:** Investigating the collective behavior of an ensemble of interacting ABPs within FCDs. How do particle-particle interactions (e.g., excluded volume, hydrodynamic interactions) combine with the guiding effect of the FCDs to produce emergent patterns or large-scale transport?

- **Different types of active particles:** Exploring the dynamics of other types of active particles, such as active colloids with different surface anchoring conditions (e.g., homeotropic, planar, Janus), which would dictate how they interact with the liquid crystal director and potentially lead to different self-propulsion mechanisms relative to the director.

- **Connection to experiments:** Collaborating with experimentalists to compare simulation results with real-world observations of active particles in smectic liquid crystals. This could help validate the model and guide future theoretical developments.

This work provides a foundational understanding of active particle transport in structured smectic liquid crystal environments. By pursuing these future directions, we can further unravel the complex and fascinating physics of active matter in anisotropic soft media, paving the way for potential applications in microfluidics, active material design, and targeted delivery systems.

Appendix A

Generation of Synthetic Smectic-A Director Fields

This appendix provides a brief explanation of how a specific type of synthetic smectic-A (SmA) director field was generated using the Python language. For mimetic FCDs, the implementation, as detailed below, generates a periodic textured field based on a simple potential function. This explanation aims to clarify the computational process and the underlying mathematical operations.

A.0.1 Purpose of the Algorithm

The algorithm is designed to create a 2D director field $\hat{\mathbf{n}}(x, y) = (n_x, n_y)$ across a square grid of size $N \times N$. It also returns a potential function $\phi(x, y)$, which can be conceptually related to the smectic layer positions.

The fundamental principle employed for generating the director field is based on the relationship between smectic layers and the director. In an ideal smectic phase, the director field $\hat{\mathbf{n}}$ is everywhere perpendicular to the smectic layers. If the layers can be described by surfaces of constant phase $\phi(\vec{r})$, then the director is given by the normalized gradient of this phase function, $\hat{\mathbf{n}} = \nabla\phi/|\nabla\phi|$. Our algorithm takes advantage of this concept by defining a specific periodic function ϕ in the simulation domain.

The computational steps are as follows:

1. **Grid initialization:** The function first initializes a 2D grid of coordinates (X, Y) that span the simulation box of linear dimension N.

2. **Periodic potential $\phi(x, y)$ generation:** The core of the director field generation lies in defining a periodic potential function $\phi(X, Y)$. To create periodicity, the coordinates are first normalized x_{norm} and y_{norm}. These normalized coordinates are then used to define the potential function $\phi(x, y)$ according

to a simple sum of cosine waves:

$$\phi(x, y) = \cos(x_{\text{norm}}) + \cos(y_{\text{norm}}) \tag{A.1}$$

This function creates a 2D periodic landscape, where constant ϕ contours resemble a grid.

3. **Director field calculation from gradient:** The director field $\hat{\mathbf{n}} = (n_x, n_y)$ is derived from the gradient of ϕ. The components of the gradient vector, $\nabla_x\phi$ and $\nabla_y\phi$, are computed numerically using the Numpy's gradient function.

   The magnitude of the gradient vector is then calculated $|\nabla\phi|$.

   To prevent division by zero in regions where the gradient might vanish (e.g., at the peaks or troughs of the cosine waves where ϕ has local extrema), a small regularization constant (10^{-10}) is applied:

   $$|\nabla\phi|_{\text{reg}} = \max(|\nabla\phi|, 10^{-10})$$

   Finally, the director components n_x and n_y are obtained by normalizing the gradient vector:

   $$n_x = \frac{\nabla\phi_x}{|\nabla\phi|_{\text{reg}}}$$
   $$n_y = \frac{\nabla\phi_y}{|\nabla\phi|_{\text{reg}}}$$

4. **Output:** The function returns a dictionary $\hat{\mathbf{n}}$ containing the calculated x and y components of the director field for each point on the grid, and the potential ϕ itself.

It is important to understand the specific characteristics of the director field generated by our algorithm. The implementation (specifically the calculation of ϕ in Eq. (A.1)) generates a periodic director field with a square lattice of topological defects. These defects correspond to alternating $+1$ and -1 defects in the phase field, often associated with splay and bend distortions. This differs significantly from the geometrically precise FCDs with point singularities (see Figure 3.5a).

Furthermore, several parameters related to the FCD tiling and local coordinates are defined within the algorithm but are not directly used in the final calculation of the n_x and n_y components that define the returned $\hat{\mathbf{n}}$. Additionally, the total

director angle variable, which appears to intend to add a uniform background director, is also not incorporated into the final $\hat{\mathbf{n}}$ returned by our algorithm. Finally, many loops are made, meaning the algorithm will only execute the loop once and return the field for the entire $N \times N$ grid (as ϕ is calculated globally), rather than tiling multiple distinct FCDs.

Therefore, this algorithm provides a synthetic, periodic smectic-like texture useful for exploring ABP dynamics in a structured, non-uniform environment, but it does not accurately reproduce the complex layer geometry and defect structure characteristic of true FCD.

Bibliography

[1] Igor Aranson. The aquatic dance of bacteria. *Physics*, 6:61, 2013.

[2] Igor S Aranson. Harnessing medium anisotropy to control active matter. *Accounts of chemical research*, 51(12):3023–3030, 2018.

[3] Clemens Bechinger, Roberto Di Leonardo, Hartmut Löwen, Charles Reichhardt, Giorgio Volpe, and Giovanni Volpe. Active particles in complex and crowded environments. *Reviews of modern physics*, 88(4):045006, 2016.

[4] Andrew Berdahl, Colin J Torney, Christos C Ioannou, Jolyon J Faria, and Iain D Couzin. Emergent sensing of complex environments by mobile animal groups. *Science*, 339(6119):574–576, 2013.

[5] P Boltenhagen, M Kleman, and OD Lavrentovich. Focal conics domains in smectics. In *Soft Order in Physical Systems*, pages 5–32. Springer, 1994.

[6] Robert Brown. *The Miscellaneous Botanical Works of Robert Brown: Vol. I*. BoD–Books on Demand, 2022.

[7] L Bruno and MA Despósito. Analytical description of anomalous diffusion in living cells. *arXiv preprint arXiv:0904.2133*, 2009.

[8] Michael E Cates and Julien Tailleur. Motility-induced phase separation. *Annu. Rev. Condens. Matter Phys.*, 6(1):219–244, 2015.

[9] Paul M Chaikin, Tom C Lubensky, and Thomas A Witten. *Principles of condensed matter physics*, volume 10. Cambridge university press Cambridge, 1995.

[10] Pierre-Gilles De Gennes and Jacques Prost. *The physics of liquid crystals*. Number 83. Oxford university press, 1993.

[11] Stephen J Ebbens and Jonathan R Howse. In pursuit of propulsion at the nanoscale. *Soft Matter*, 6(4):726–738, 2010.

[12] Claudia Ferreiro-Córdova, John Toner, Hartmut Löwen, and Henricus H Wensink. Long-time anomalous swimmer diffusion in smectic liquid crystals. *Physical Review E*, 97(6):062606, 2018.

[13] Crispin W Gardiner. Handbook of stochastic methods for physics, chemistry and the natural sciences. *Springer series in synergetics*, 1985.

[14] Peter Hänggi and Fabio Marchesoni. Introduction: 100years of brownian motion. *Chaos: An Interdisciplinary Journal of Nonlinear Science*, 15(2), 2005.

[15] Maurice Kleman and Oleg D Lavrentovich. *Soft matter physics: an introduction*. Springer, 2003.

[16] Ryogo Kubo. Brownian motion and nonequilibrium statistical mechanics. *Science*, 233(4761):330–334, 1986.

[17] Danilo B Liarte, Matthew Bierbaum, Muxin Zhang, Brian D Leahy, Itai Cohen, and James P Sethna. Visualization, coarsening, and flow dynamics of focal conic domains in simulated smectic-a liquid crystals. *Physical Review E*, 92(6):062511, 2015.

[18] M Cristina Marchetti, Jean-François Joanny, Sriram Ramaswamy, Tanniemola B Liverpool, Jacques Prost, Madan Rao, and R Aditi Simha. Hydrodynamics of soft active matter. *Reviews of modern physics*, 85(3):1143–1189, 2013.

[19] Oleg F Petrov, Roman E Boltnev, and Mikhail M Vasiliev. Experimental evolution of active brownian grains driven by quantum effects in superfluid helium. *Scientific Reports*, 12(1):6085, 2022.

[20] Sriram Ramaswamy. The mechanics and statistics of active matter. *Annu. Rev. Condens. Matter Phys.*, 1(1):323–345, 2010.

[21] Pawel Romanczuk, Markus Bär, Werner Ebeling, Benjamin Lindner, and Lutz Schimansky-Geier. Active brownian particles: From individual to collective stochastic dynamics. *The European Physical Journal Special Topics*, 202:1–162, 2012.

[22] Timothy J Rudge and et al. Federici. Cell polarity-driven instability generates self-organized, fractal patterning of cell layers. *ACS synthetic biology*, 2(12):705–714, 2013.

[23] Andrey Sokolov, Shuang Zhou, Oleg D Lavrentovich, and Igor S Aranson. Individual behavior and pairwise interactions between microswimmers in anisotropic liquid. *Physical Review E*, 91(1):013009, 2015.

[24] Tânia Tomé. *Dinâmica Estocástica e Irreversibilidade Vol. 35*. Edusp, 2001.

[25] John Toner, Hartmut Löwen, and Henricus H Wensink. Following fluctuating signs: Anomalous active superdiffusion of swimmers in anisotropic media. *Physical Review E*, 93(6):062610, 2016.

[26] Rishi R Trivedi, Rina Maeda, Nicholas L Abbott, Saverio E Spagnolie, and Douglas B Weibel. Bacterial transport of colloids in liquid crystalline environments. *Soft Matter*, 11(43):8404–8408, 2015.

[27] Nicolaas Godfried Van Kampen. *Stochastic processes in physics and chemistry*, volume 1. Elsevier, 1992.

[28] Tamás Vicsek and Anna Zafeiris. Collective motion. *Physics reports*, 517(3-4):71–140, 2012.

[29] Angel Daniel Viñales and Marcelo Arnaldo Desposito. Anomalous diffusion: Exact solution of the generalized langevin equation for harmonically bounded particle. *Physical Review E—Statistical, Nonlinear, and Soft Matter Physics*, 73(1):016111, 2006.

[30] Andreas Walther and Axel HE Muller. Janus particles: synthesis, self-assembly, physical properties, and applications. *Chemical reviews*, 113(7):5194–5261, 2013.

[31] Shuang Zhou, Oleh Tovkach, Dmitry Golovaty, Andrey Sokolov, Igor S Aranson, and Oleg D Lavrentovich. Dynamic states of swimming bacteria in a nematic liquid crystal cell with homeotropic alignment. *New Journal of Physics*, 19(5):055006, 2017.